Deep Earth materials, structure and dynamics: eleven **major developments in the CEED decade**. A personal (re)view.

Deep Earth group: focus on the lower mantle (LM) and outer core - and especially:

- the lowermost mantle thermal boundary layer (D’’) with LLSVPs and ULVZs
- probable Hadean refractory and bridgmanitic domains in the mid-LM
- chemical exchange between an initial magma ocean (MO) and protocore and subsequent basal MO (BMO) and core, which has consequences for the composition and structure of LM and outermost core (E'-layer)

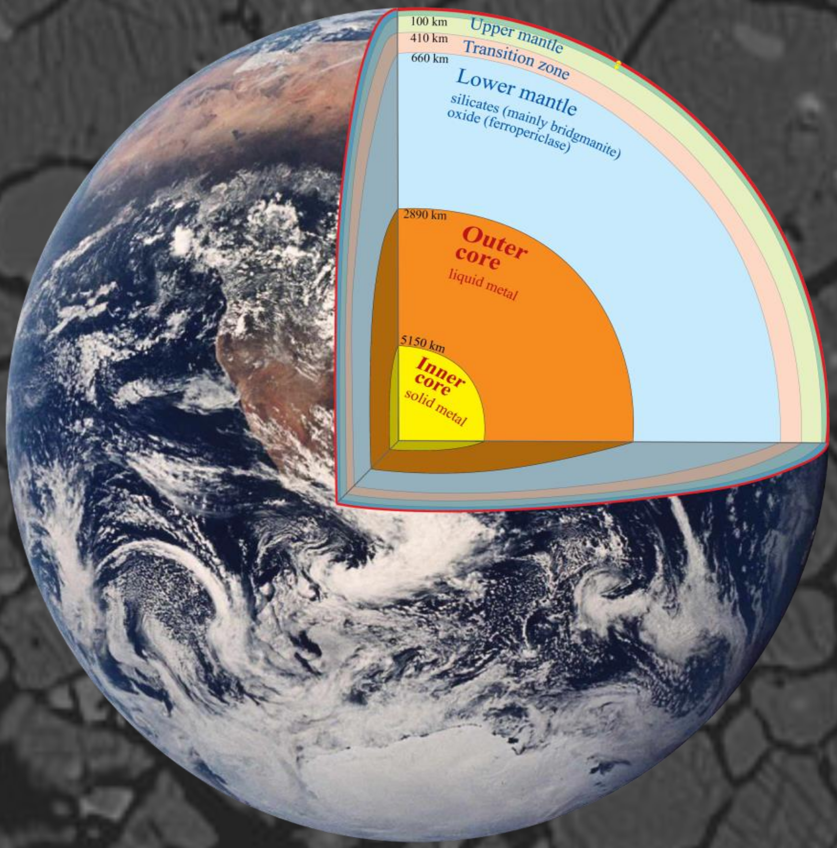

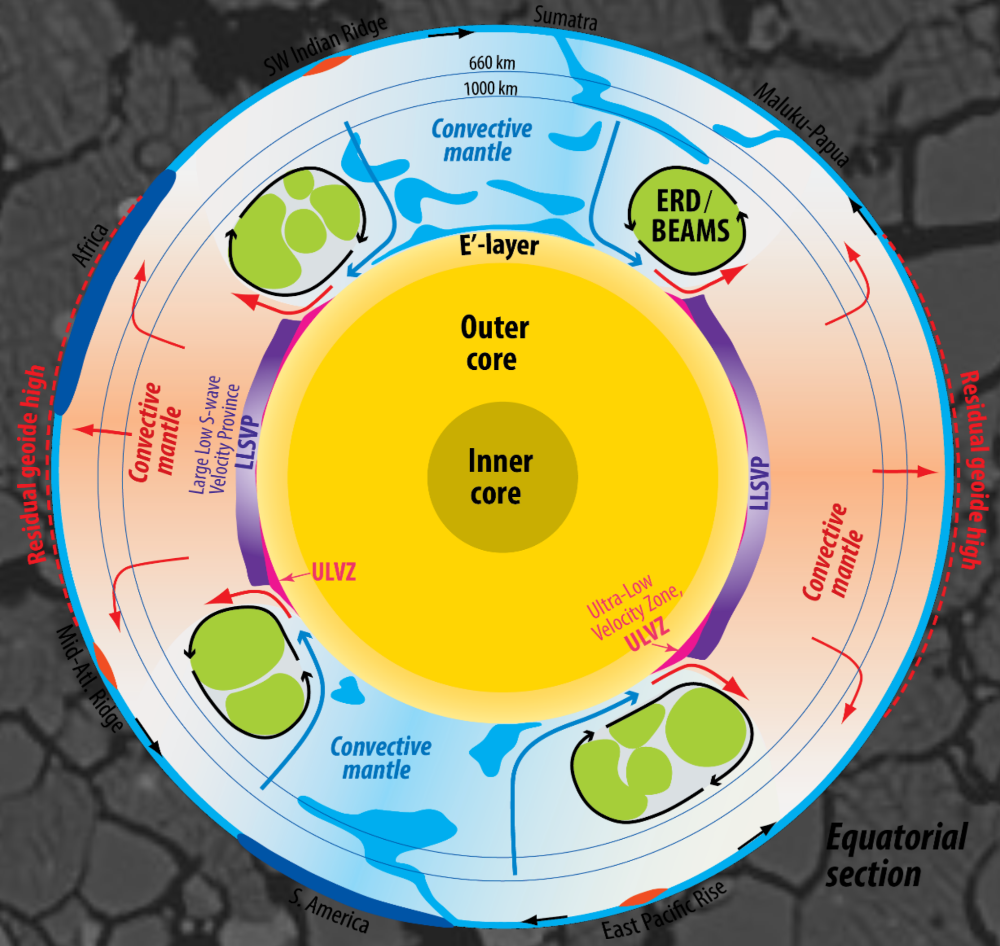

Major developments in deep Earth materials and dynamics in the CEED decade

Divided into two themes:

- **Phase relations and density** (8 topics)

- **Degree-2 residual geoid, LM viscosity and LLSVP base layer thickness and density excess** (3 topics)

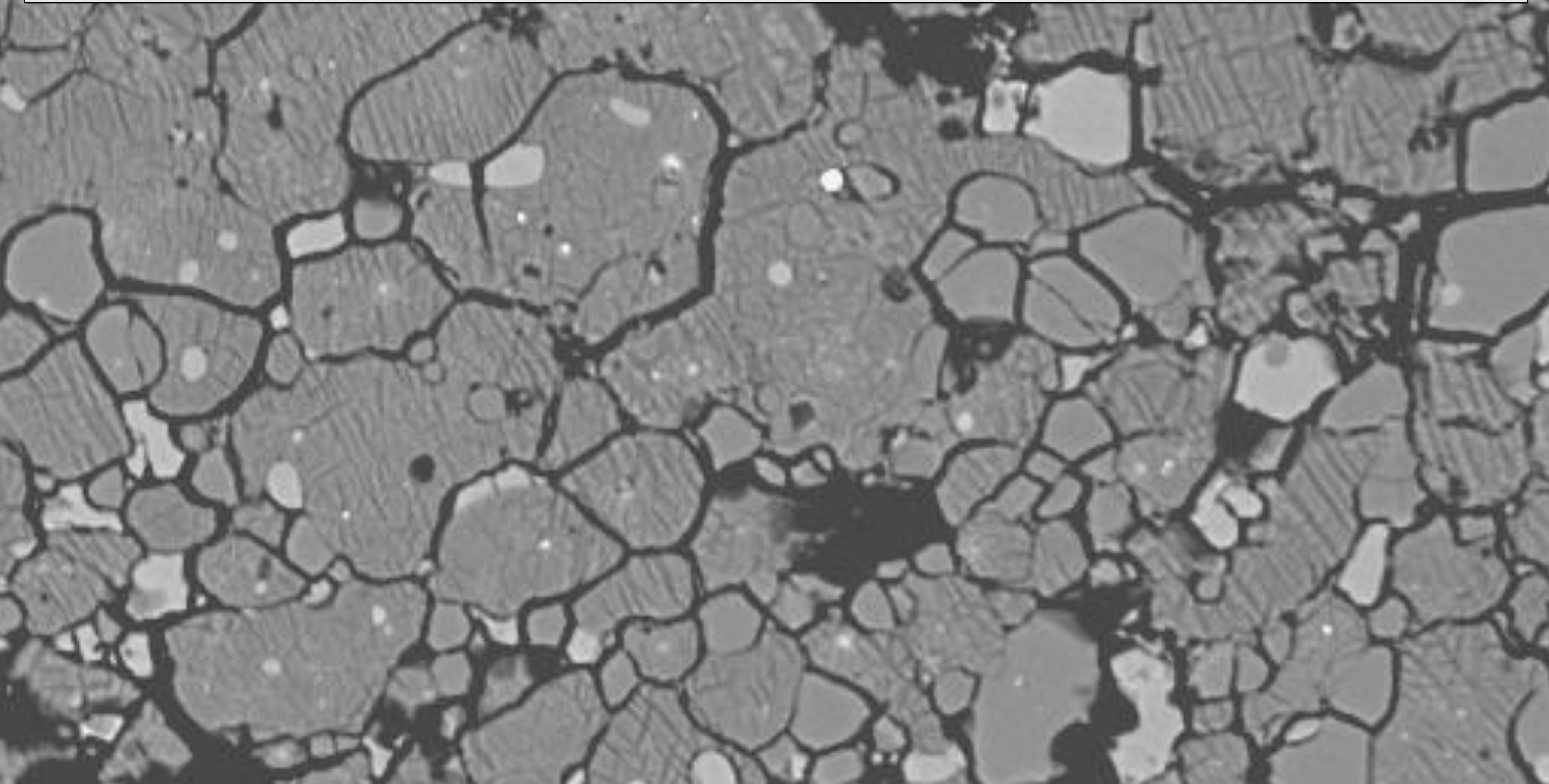

Strengthened case for a long-lived basal magma ocean (BMO) – possibly to the late Proterozoic?? (Labrosse et al. 2007, Nat)

Strong Fe-partitioning from bridgmanite (bm) to melt (e.g. Tateno et al. 2014, JGR), which densifies melts during fractionstion

Bm-melt and periclase-melt density relations for $MgSiO_3$ and MgO (Petitgirard et al. 2015, PNAS, Ghosh & Karki 2016)

Bm-melt density relations in peridotitic systems (**Caracas** et al. 2019, JGR; **Trønnes** et al. 2019, Tectonoph)

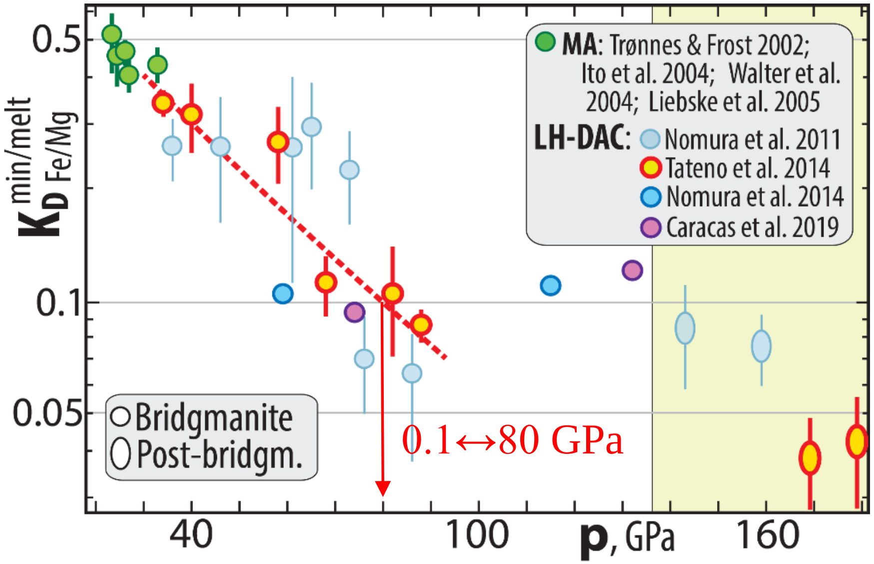

$$K_{D\ Fe/Mg}^{bm/melt} = (Fe/Mg)^{bm} / (Fe/Mg)^{melt}$$

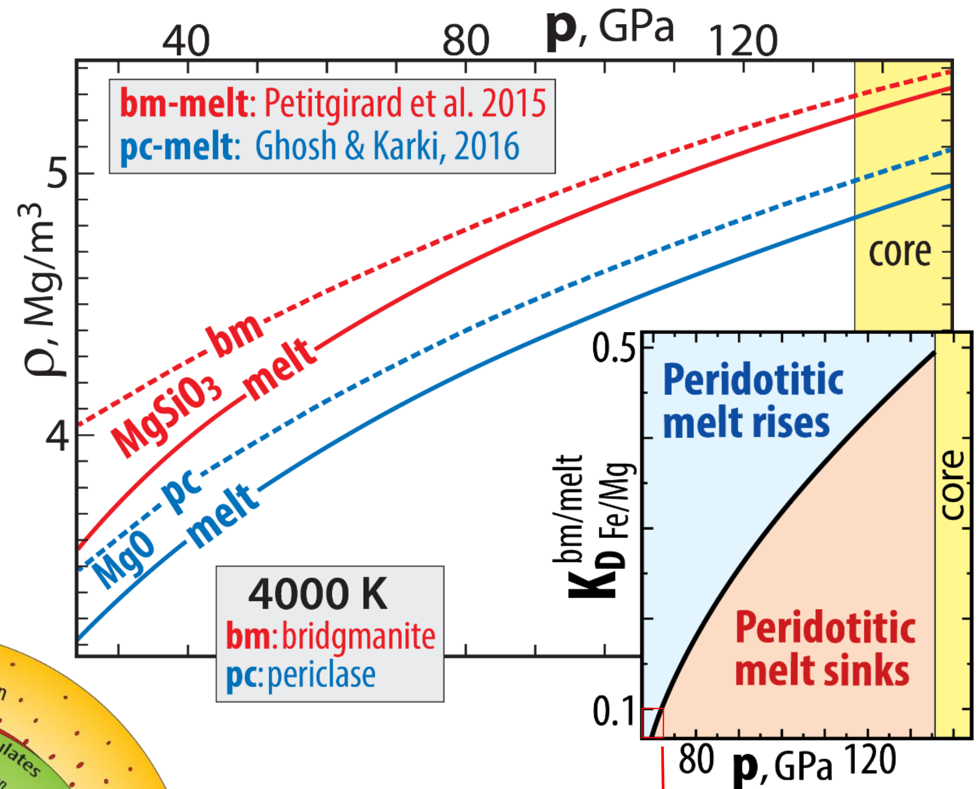

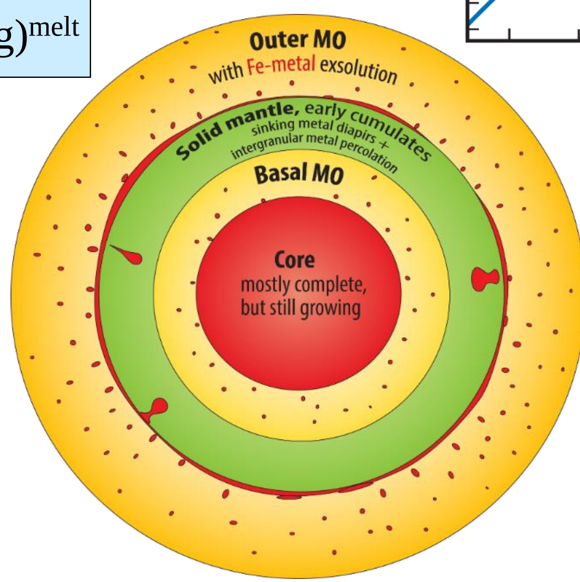

Neutral buoyancy for

$K_D = 0.1 \rightarrow 73$ GPa

73-80 GPa,

~1800 km depth

(PREM)

Chemical exchange, core-BMO and the implications for outermost core (E'-layer) and LM

Light element composition of the outer core from mineral physics (Badro, Coté, **Brodholt** 2015, PNAS; Badro, **Brodholt** et al. 2014, PNAS)

Evidence that the outer core alloy is O-undersaturated → FeO from bm and ferropericlase to the core (Takafuji et al. 2005; Frost et al. 2010)

Geophysical constraints on E'-layer (Lay & Young, 1990, GRL; Garnero et al. 1993, GRL; Helffrich & Kaneshima 2010, Nature; Kaneshima & Helffrich, 2013, GJI; Kaneshima, 2018, PEPI; Irving et al. 2018. Sci Adv)

Core-BMO exchange: SiO_2↔FeO, E'-layer (**Brodholt** & Badro 2017, GRL; Hirose et al. 2017, Nat; **Trønnes et al.** 2019, Tectonoph; Helffrich et al. 2020)

Fairly large and complex topic - if interested, see recorded lecture at:

www.nhm.uio.no/english/about/organization/research-collections/people/rtronnes/1/other-lect/sem-mtg/Core-MO-exchange-Rec.pptx

Trønnes-UiO-page → Teaching → other-lect → sem-mtg → Core-MO-exchange-Rec.pptxZ

Metal-silicate exchange equilibrium leading to **core - BMO** chemical exhange during cooling

$$2\,Fe^{met} + SiO_2^{sil} = Si^{met} + 2\,FeO^{sil}$$

displaced towards the products with **increasing T**
and reversed during **cooling**

Large terrestrial planets Venus & Earth:
core segregation at **very high T**, allowing
high $Si^{protocore}$ **and** high FeO^{MO} (i.e. high f_{O_2})

Cooling ⇨ core-BMO **chemical exchange**

- FeO and $FeO_{1.5}$ from BMO to the core
- SiO_2 from core to BMO

Plume flux and core-to-plume-contamination of W, presumably via ULVZs, **but not** He and Ne

Correlation: plume flux, $^3He/^4He$- and $^{182}W/^{184}W$-ratios (Jackson et al. 2017, Hoggard et al. 2020, EPSL; Bao et al. 2022, Sci, Mundl et al. 2017, Sci)

In spite of this: primordial He-Ne-signal is **not** from core. Met-sil partitioning predicts too high He/Ne core (Li, **Brodholt** et al. 2022, Nat Comm)

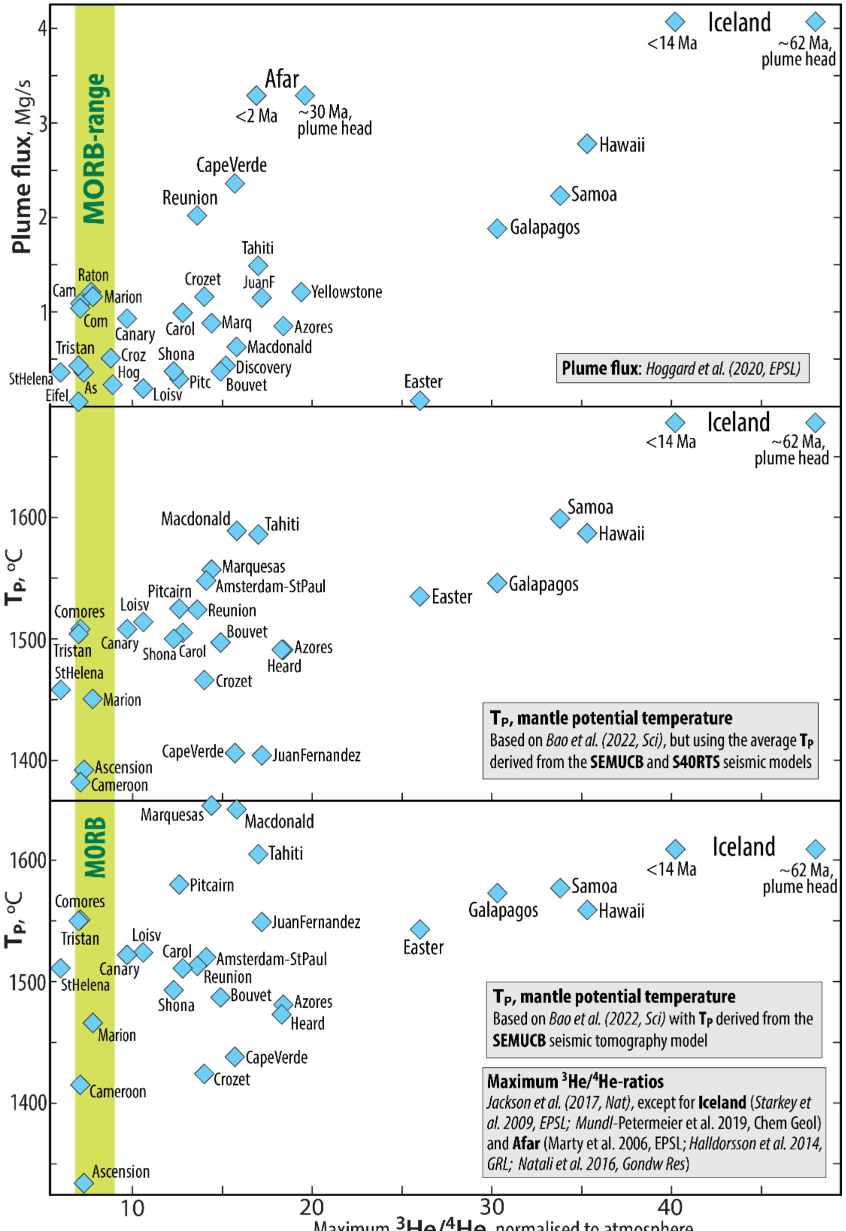

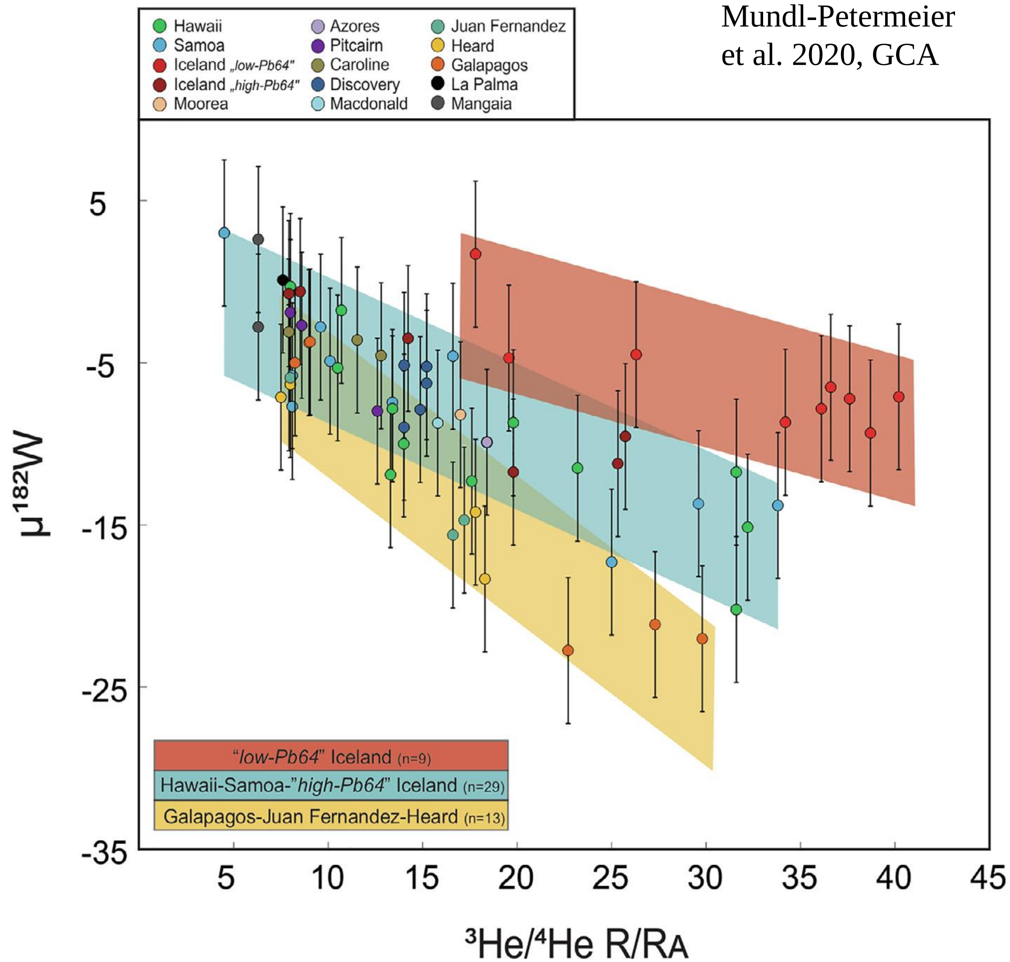

Mundl-Petermeier et al. 2020, GCA

Early refractory domains (ERDs) are bridgmanitic, Hadean and likely sources of primordial-like He- and Ne-isotopic signatures.

Geodynamic BEAMS-model (Ballmer et al. 2017, NG). Tenuous seismic evidence for ferropericlase-free domains (**Shephard** et al. 2021, NC)

He-Ne-diffusion rates in bm supports primordial signal from Hadean refractory BEAMS, (**Trønnes** et al. in prep)

Ballmer et al. (2017, Nat Geosci): BEAMS-modelling

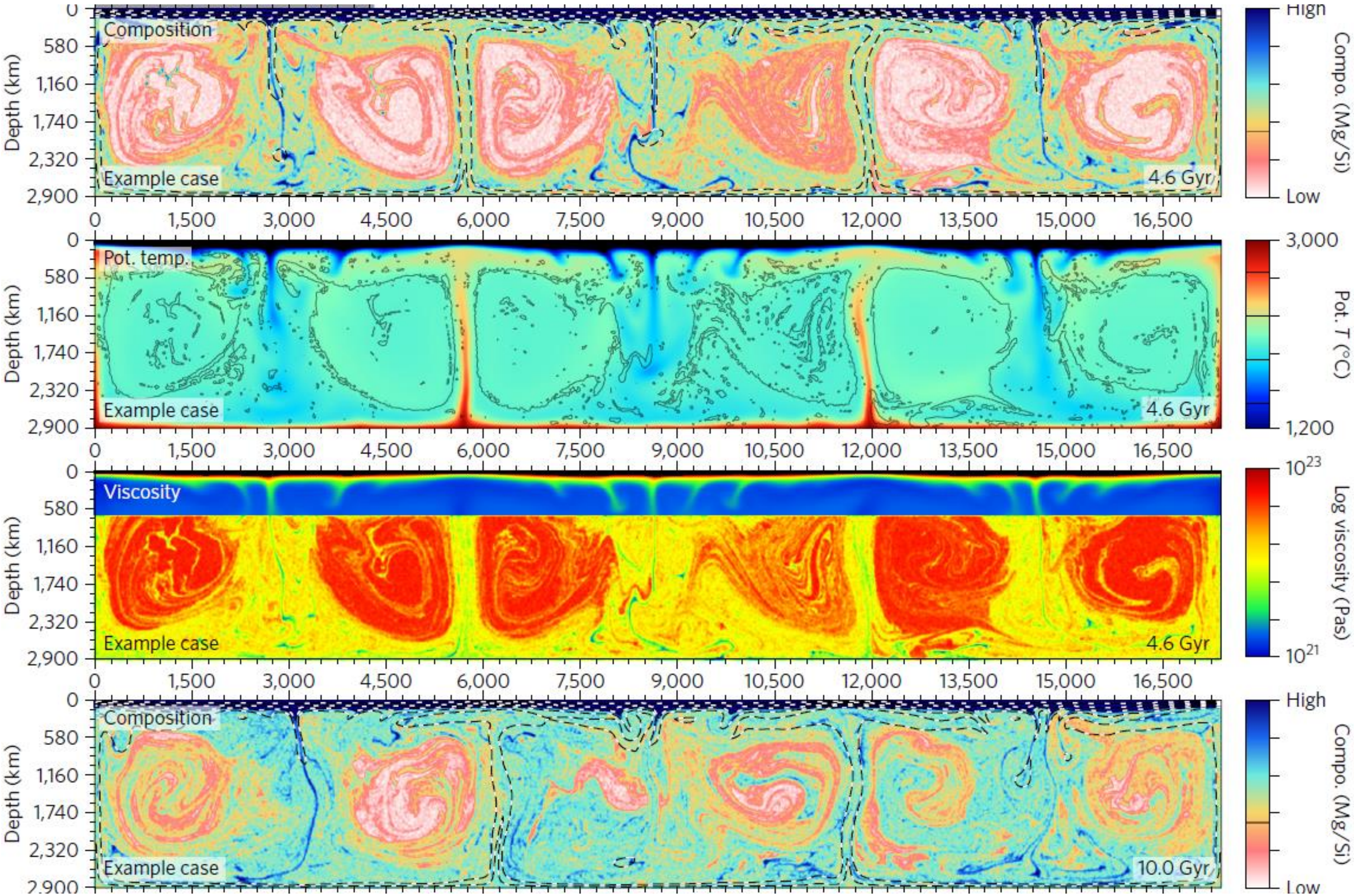

Early refractory domains. ERDs: bridgmanitic, Hadean and likely sources of primordial-like He- and Ne-isotopic signatures)

Geodynamic BEAMS-model (Ballmer et al. 2017, NG). Tenuous seismic evidence for ferropericlase-free domains (**Shephard** et al. 2021, NC)

He-Ne-diffusion rates in bm supports primordial signal from Hadean refractory BEAMS, (**Trønnes** et al. in prep)

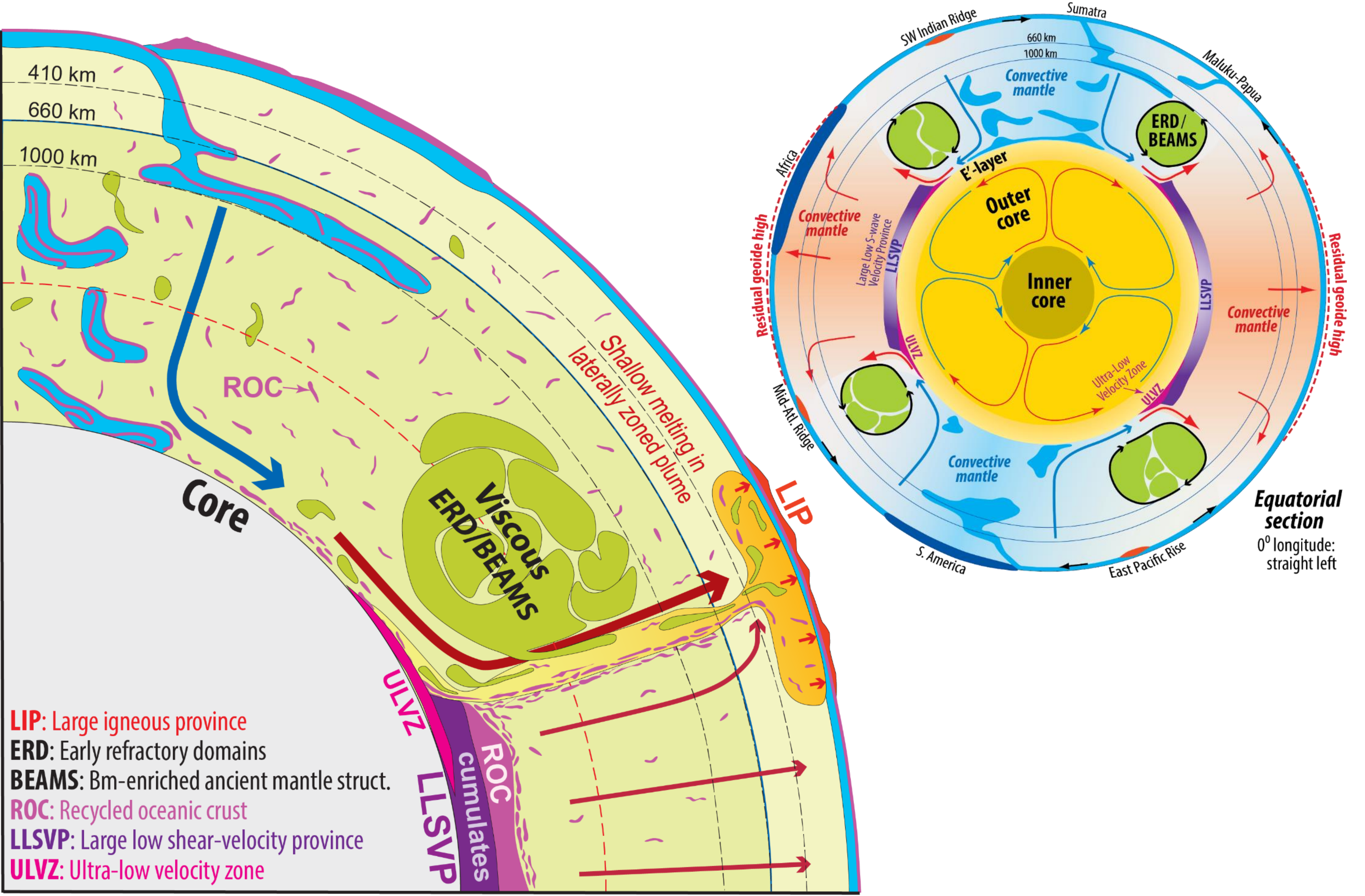

Diffusion length scales for He and Ne in bm at **about 1800 km depth**

Trønnes et al. in prep.

Hadean. Sufficient for **He**-recharging over:

- 19 mm length scale at liquidus in 10 hr
- 10 km length scale at liquidus in 300 Ma
- 10 km length scale 100 K below solidus in 500 Ma

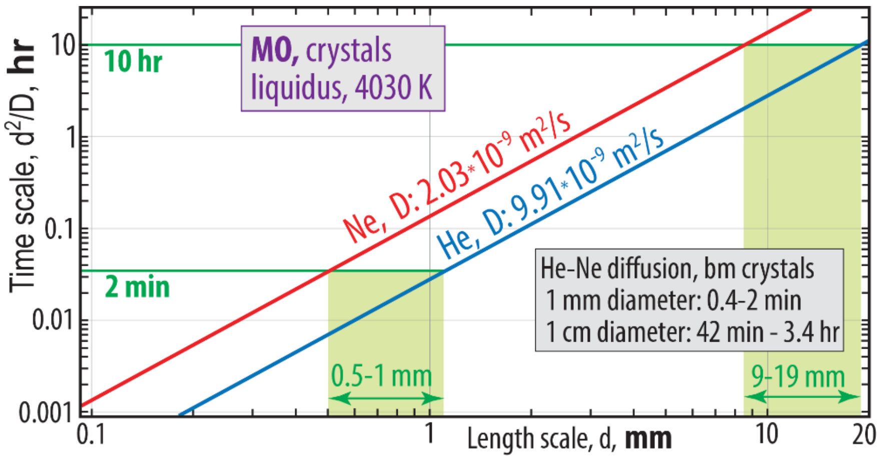

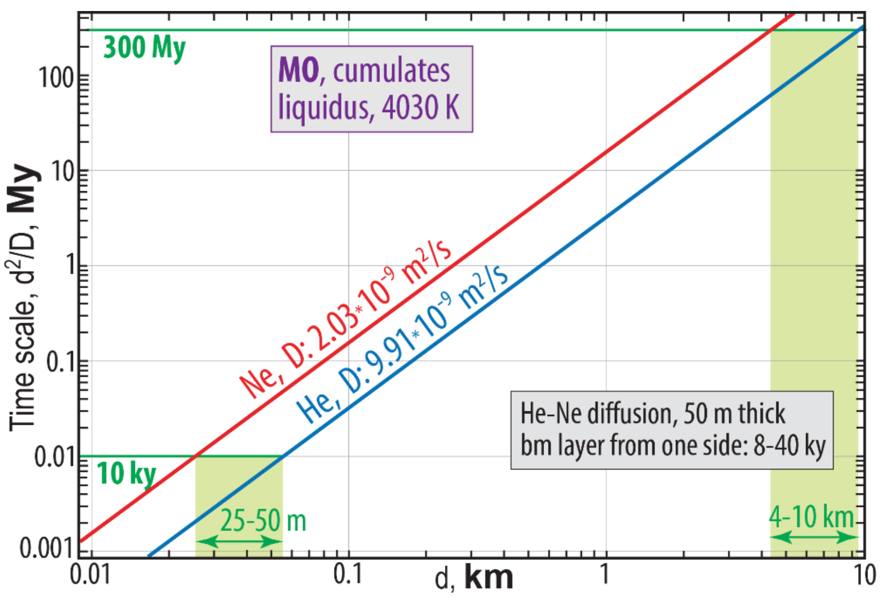

Archean-Phanerozoic

Insufficient for resetting to convective mantle **^{3}He/^{4}He** over:

>10 km length at **200 K above** the resent ambient geotherm in **4 Gy**

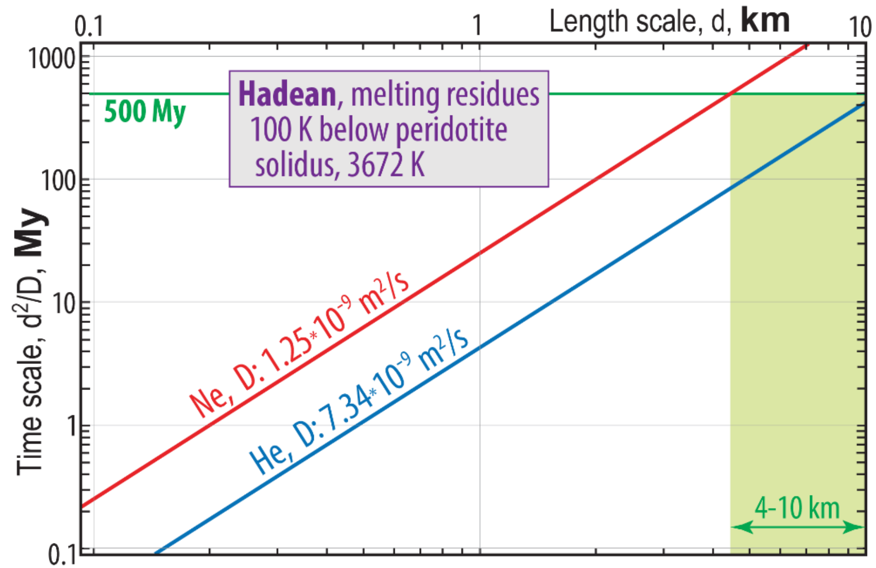

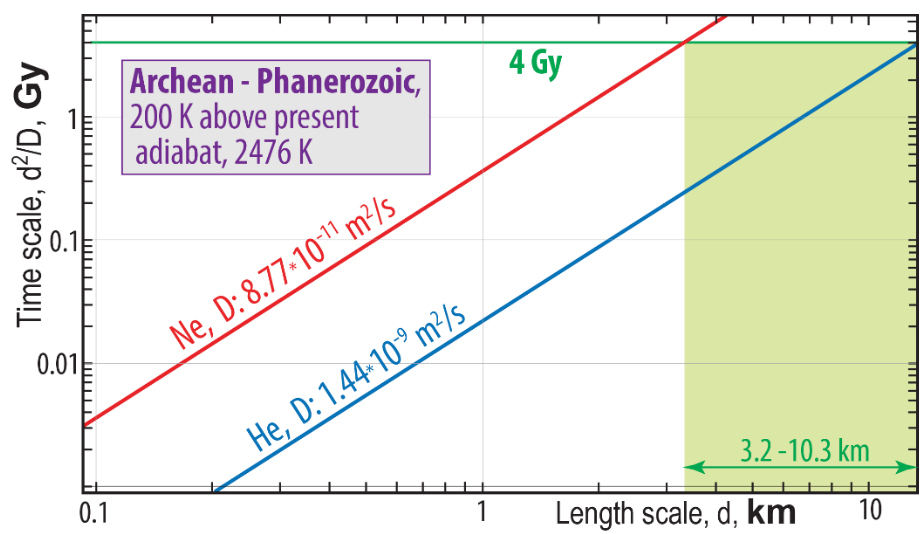

Role of dense, residual davemaoite (Ca-perovskite) in the lowermost mantle

Davemaoite-enrichment in the ULVZs from partial melting of ROC **and** in LLSVPs from MO-BMO-crystallisation.

Important implications: U-Th-enrichment and **high ^{4}He/^{3}He-** and ^{21}Ne/^{22}Ne ratios (**Hernandez** et al. 2022, GRL; **Trønnes** et al. in prep)

POSTER on Wednesday

Reduced CMB-temperature: from about 4000 to 3700 K (?), based on:

Lower melting curve for Fe at outer core conditionds (Sinmyo et al. 2019, EPSL)

Lower peridotite solidus, 3800-3600 K at the CMB (Nomura et al. 2014, Sci; Kuwayama et al. 2022, GRL; Pierru et al. 2022, EPSL)

Sinmyo et al. (2019, EPSL):
DAC-exp. with internal resistance-heating to determine the melting curve of pure Fe.

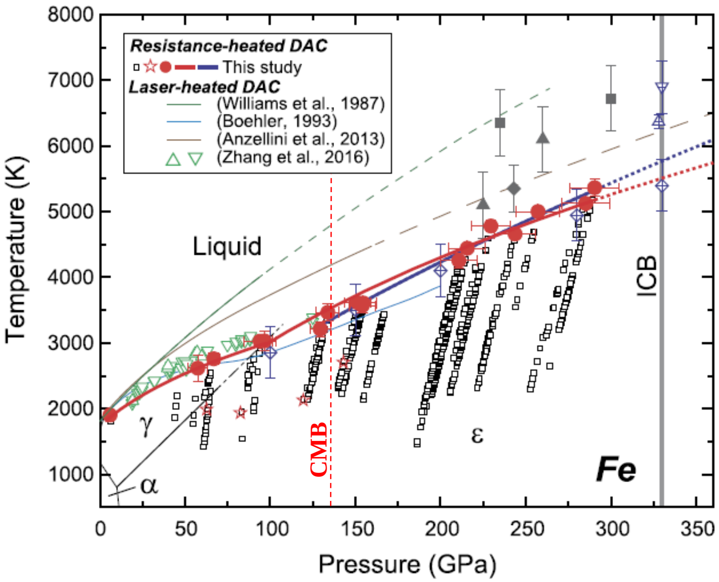

Uncertainties

Largely unknown melting curve depression due to the light element in the outer core (OC)

A main goal is to determine the ICB-T (melt ↔ solid)

The OC adiabat/geotherm would then give the CMB-T

The peridotite solidus might provide a firmer constraint.

2014-2022: several new solidus determinations: 3500-4000 K at 136 GPa

- a commonly assumed CMB-T of 4000 K is **too high**.
- we adopted the interm. Kuwayama-solidus: 3800 K and CMB-T of 3700 K.

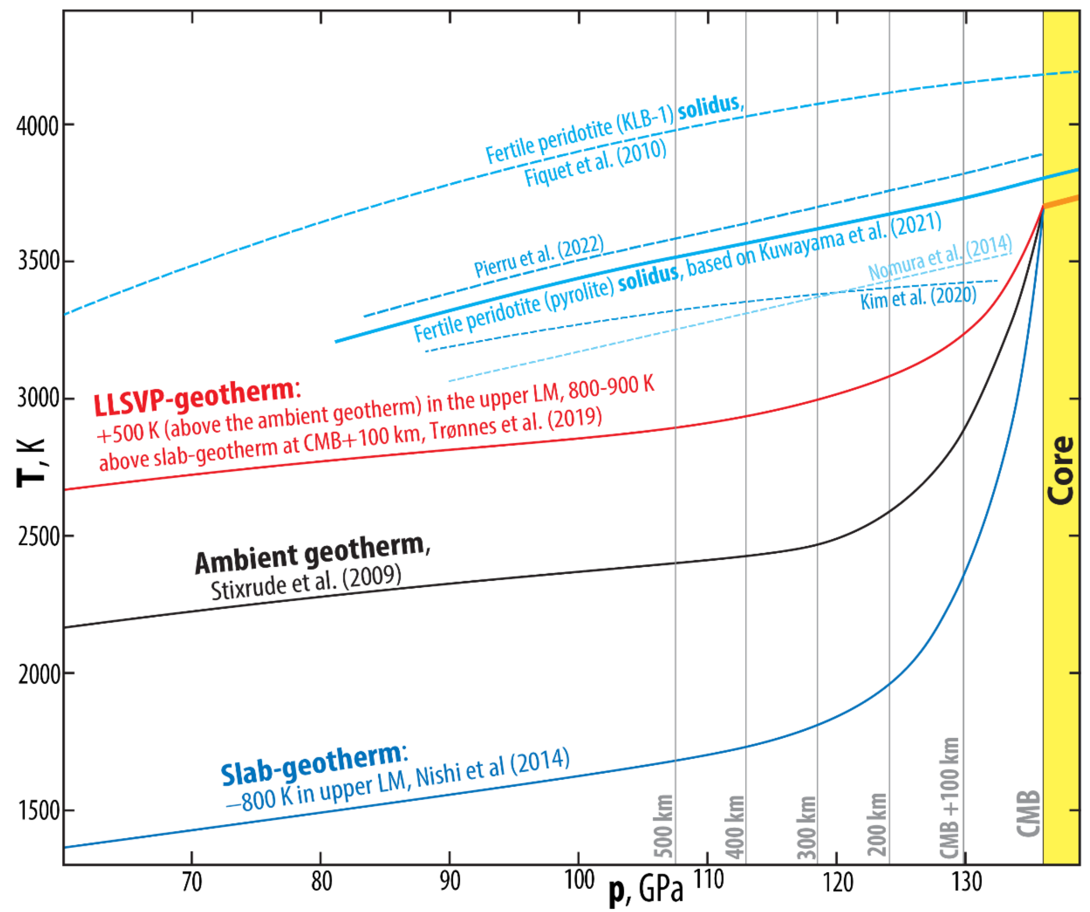

Omnipresent post-bridgmanite (pbm) in the D''-zone, and **no** double-crossing of the bm-pbm boundary, based on:

Phase relations in $MgSiO_3$(MS) - $FeSiO_3$, MS - $FeAlO_3$ and MS - Al_2O_3 (**Mohn**, in prep.; **Trønnes & Mohn**, in prep.)

Phase relations in complex peridotite (Kuwayama et al. 2022, GRL)

Reduced CMB-temperature (see above) and sharp seismic D''-discontinuity, as observed (**Mohn**, in prep.)

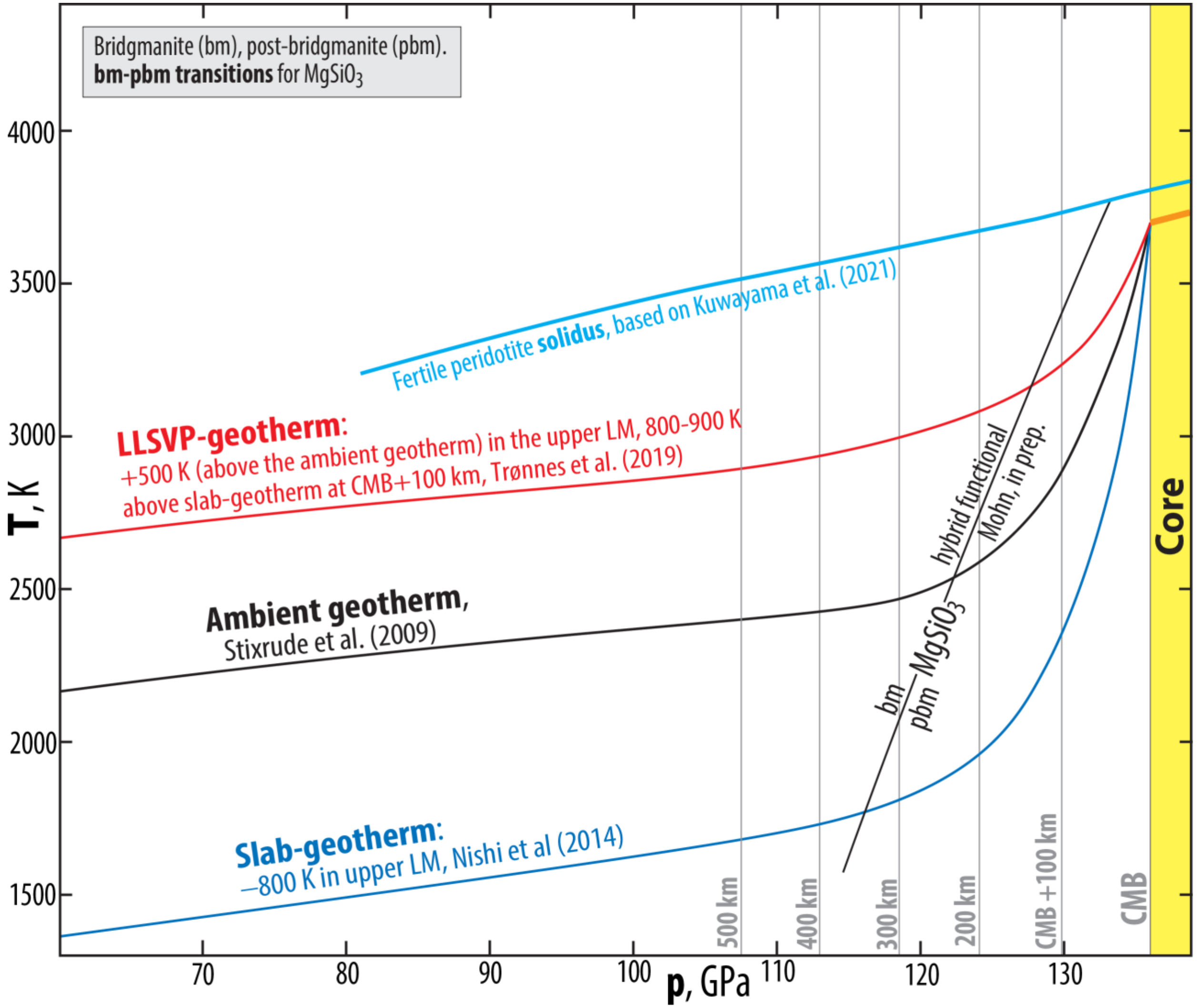

Omnipresent post-bridgmanite (pbm) in the D''-zone, **no** double-crossing of the bm-pbm boundary, based on:

Phase relations in $MgSiO_3$(MS) - $FeSiO_3$, MS - $FeAlO_3$ and MS - Al_2O_3 (**Mohn**, in prep.; **Trønnes & Mohn**, in prep.)

Phase relations in complex peridotite (Kuwayama et al. 2022, GRL)

Reduced CMB-temperature (see above) and sharp seismic D''-discontinuity, as observed (**Mohn**, in prep.)

From: Mohn (in prep.)
Stixrude & Lithgow-Bertelloni (2011, GJI)
Nagai et al. (2005, JPC)

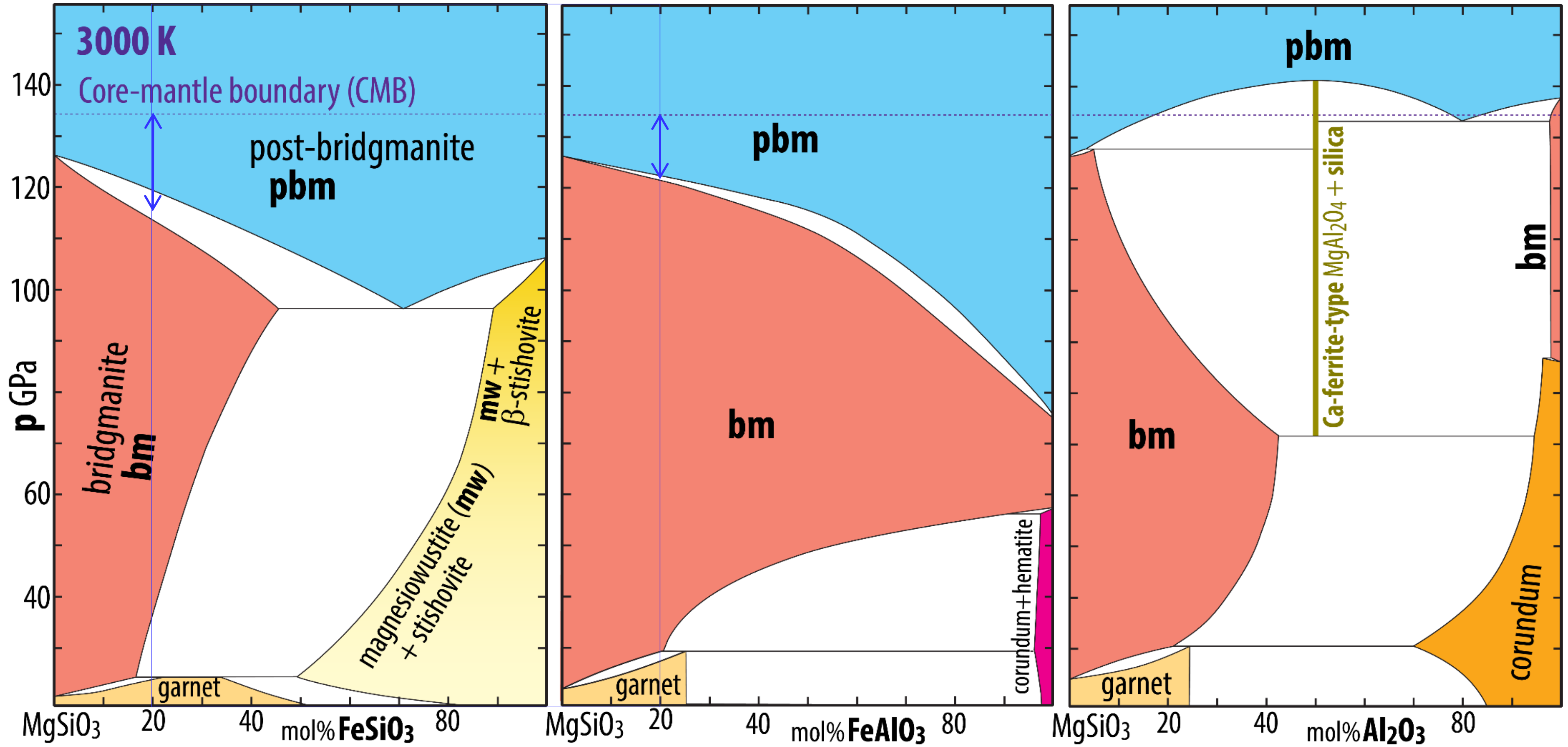

FS and FA components partition into pbm.
MS-FS phase loop is at lower p than MS-FA loop.

AA partitions into bm.
Very low Al-solubility in bm at 125 GPa.

Omnipresent post-bridgmanite (pbm) in the D"-zone, **no** double-crossing of the bm-pbm boundary, based on:

Phase relations in $MgSiO_3$(MS) - $FeSiO_3$, MS - $FeAlO_3$ and MS - Al_2O_3 (**Mohn**, in prep.; **Trønnes & Mohn**, in prep.)

Phase relations in complex peridotite (Kuwayama et al. 2022, GRL)

Reduced CMB-temperature (see above) and sharp seismic D"-discontinuity, as observed (**Mohn**, in prep.)

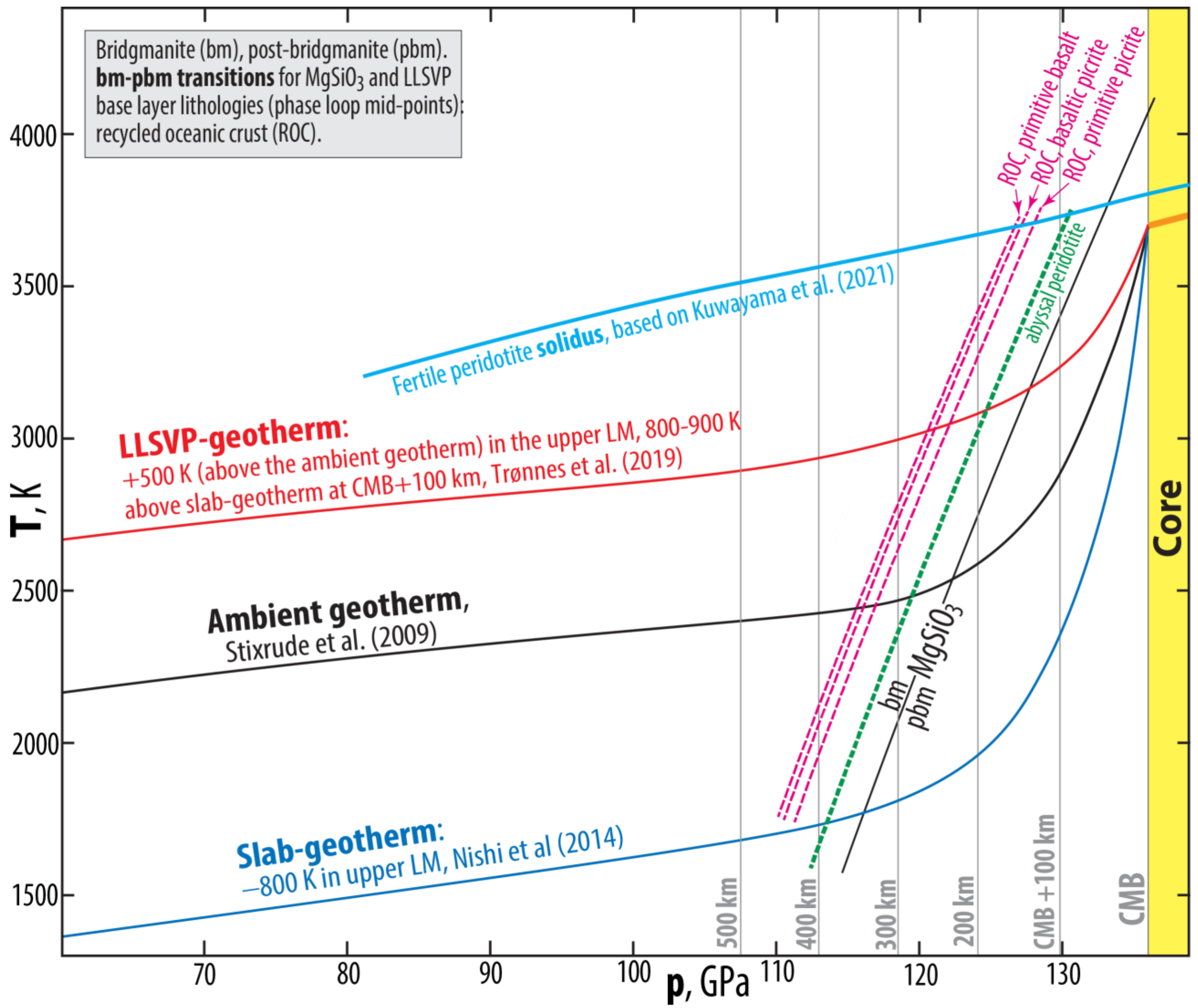

Omnipresent post-bridgmanite (pbm) in the D''-zone, **no** double-crossing of the bm-pbm boundary, based on:

Phase relations in $MgSiO_3$(MS) - $FeSiO_3$, MS - $FeAlO_3$ and MS - Al_2O_3 (**Mohn**, in prep.; **Trønnes & Mohn**, in prep.)

Phase relations in complex peridotite (Kuwayama et al. 2022, GRL)

Reduced CMB-temperature (see above) and sharp seismic D''-discontinuity, as observed (**Mohn**, in prep.)

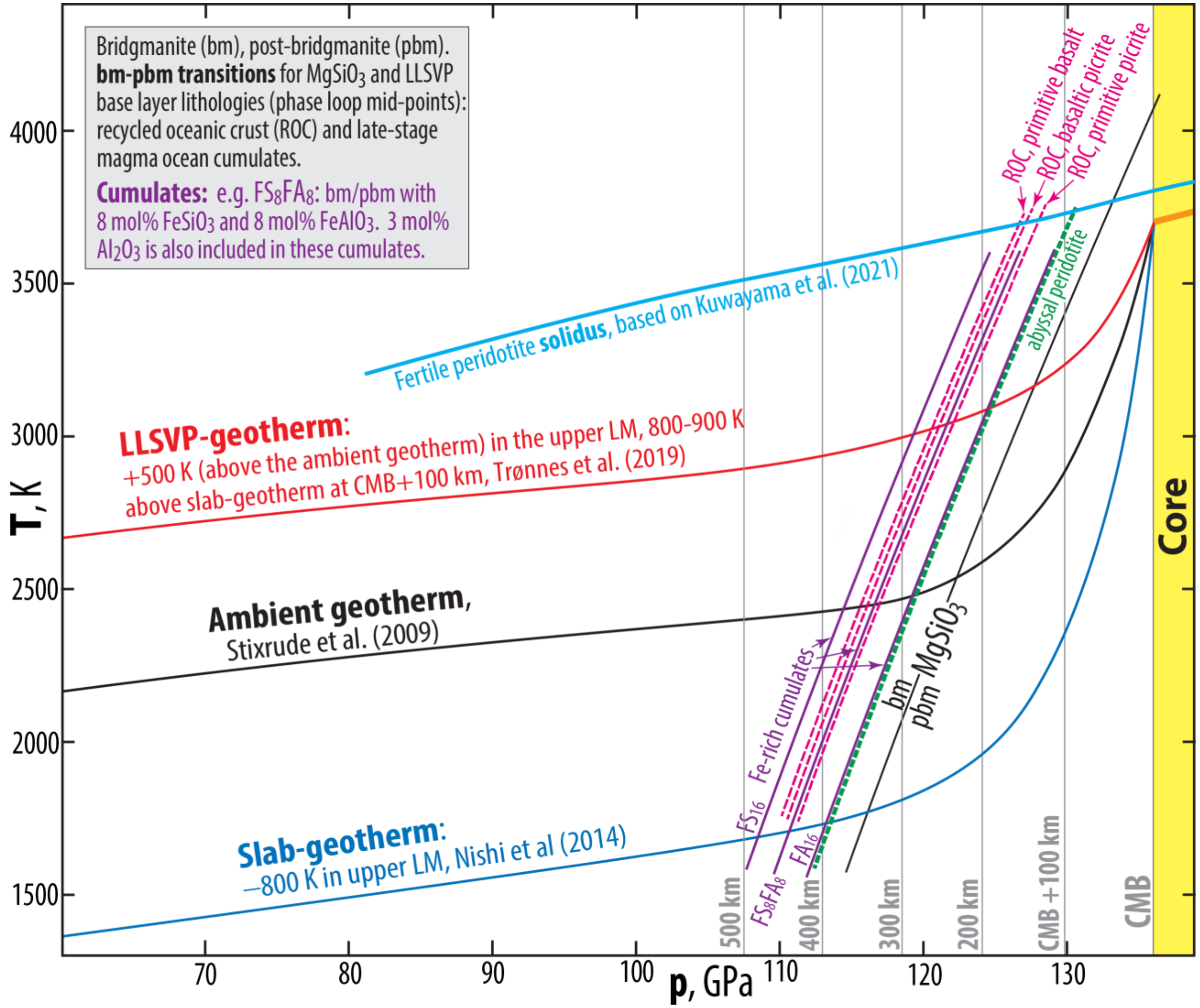

Deep subduction and recycling of upper cont. crustal slivers in the southern Gondwana hemisphere, **650**-450 Ma

Underlying density constraints at 20-27 GPa (e.g, Irifune et al. 1993; Greaux et al. 2020 and especially Ishii et al. 2012, EPSL)

Synthesis: recycling via D" with implications for the southern hemispheric DUPAL anomaly (Jackson & Macdonald 2022, AGU Adv.)

Matt Jackson will summarise some of this in less than 2 hours

UCC phase rel.,
Ishii et al. 2012

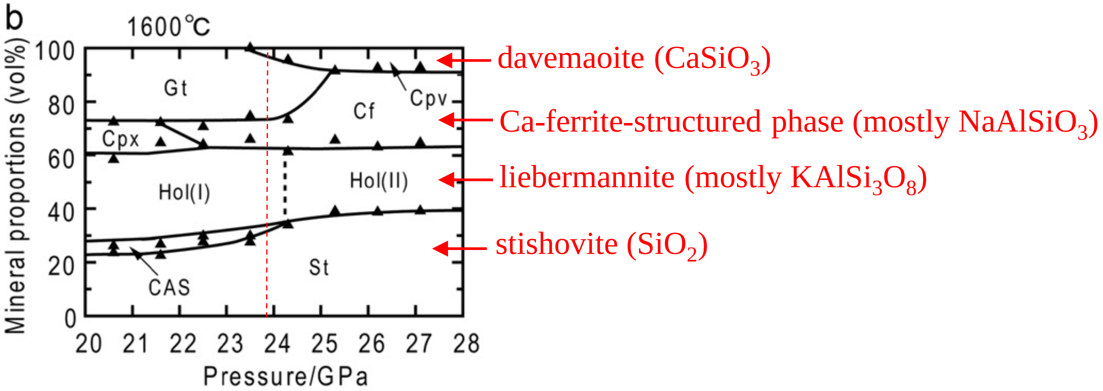

Deep subduction and recycling of upper cont. crustal slivers in the southern Gondwana hemisphere, **650**-450 Ma

Underlying density constraints at 20-27 GPa (e.g, Irifune et al. 1993; Greaux et al. 2020 and especially Ishii et al. 2012, EPSL)

Synthesis: recycling via D" with implications for the southern hemispheric DUPAL anomaly (Jackson & Macdonald 2022, AGU Adv.)

Matt Jackson will summarise some of this in less than 2 hours

UCC phase rel.
Ishii et al. 2012

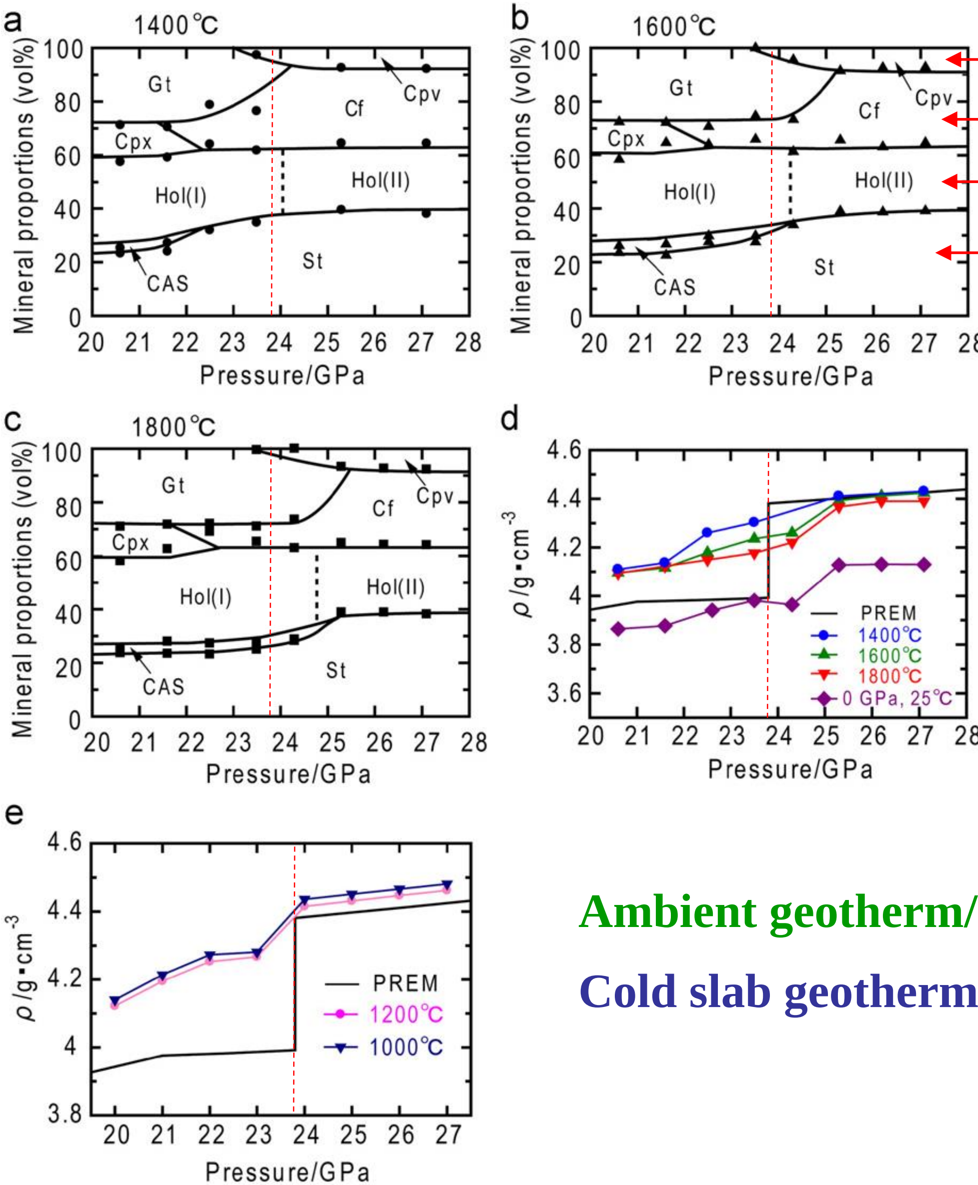

davemaoite ($CaSiO_3$)

Ca-ferrite-structured phase (mostly $NaAlSiO_3$)

liebermannite (mostly $KAlSi_3O_8$)

stishovite (SiO_2)

Ambient geotherm/adiabat: about 1600 C

Cold slab geotherm (e.g. Nishii et al. 2014): 800 C

Degree-2 residual geoid, LM viscosity and LLSVP base layer thickness and density excess

Residual geoid after subtraction of shallow slab signals (UM, MTZ) reflects a degree-2 convection pattern

Two geoid **highs** above LLSVPs, one longitudinal high-velocity belt **low** and the CMB topography reflect the degree-2 flow pattern

(e.g. Hager et al. 1985; Nat; **Steinberger & Torsvik**, 2010, GGG; **Burke** et al. 2012, GRL; Forte et al. 2015. Treat Geophys)

Hager et al. (1985)

Observed geoid

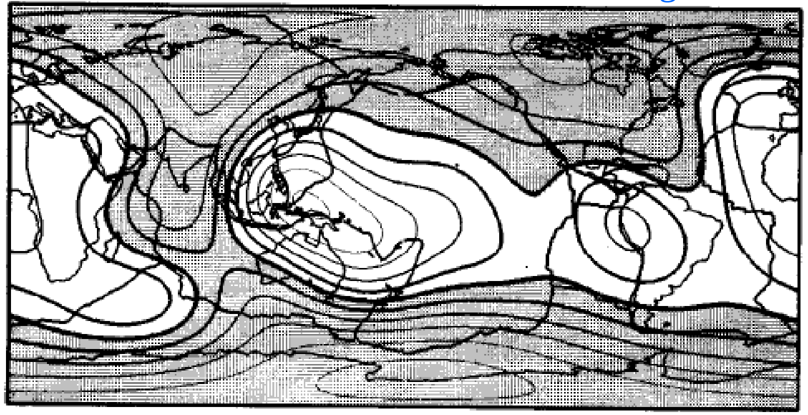

Residual geoid

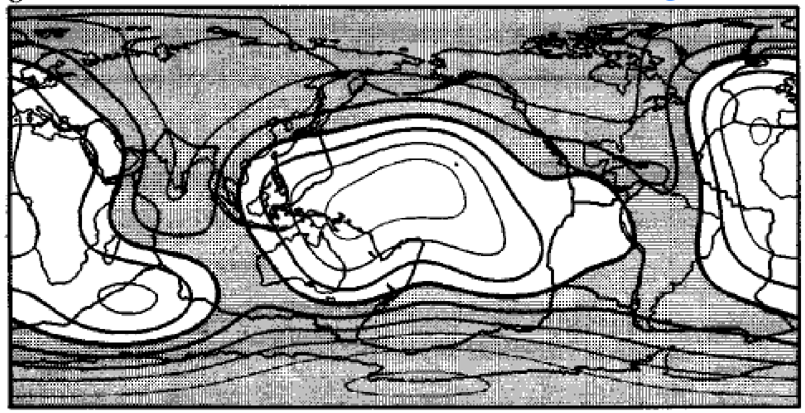

Fig. 2 *a*, The observed geoid[13] for $l = 2$–6 referred to the hydrostatic figure of the Earth. Geoid lows are shaded and the contour interval is 20 m. In all our maps, we show plate boundaries and continents for reference. *b*, The residual geoid for $l = 2$–6 obtained by subtracting the effects of subducted slabs[10]. Lows are shaded; the contour interval is 20 m.

Forte et al. (2015)

Mean CMB-topography derived from six different mantle tomography models

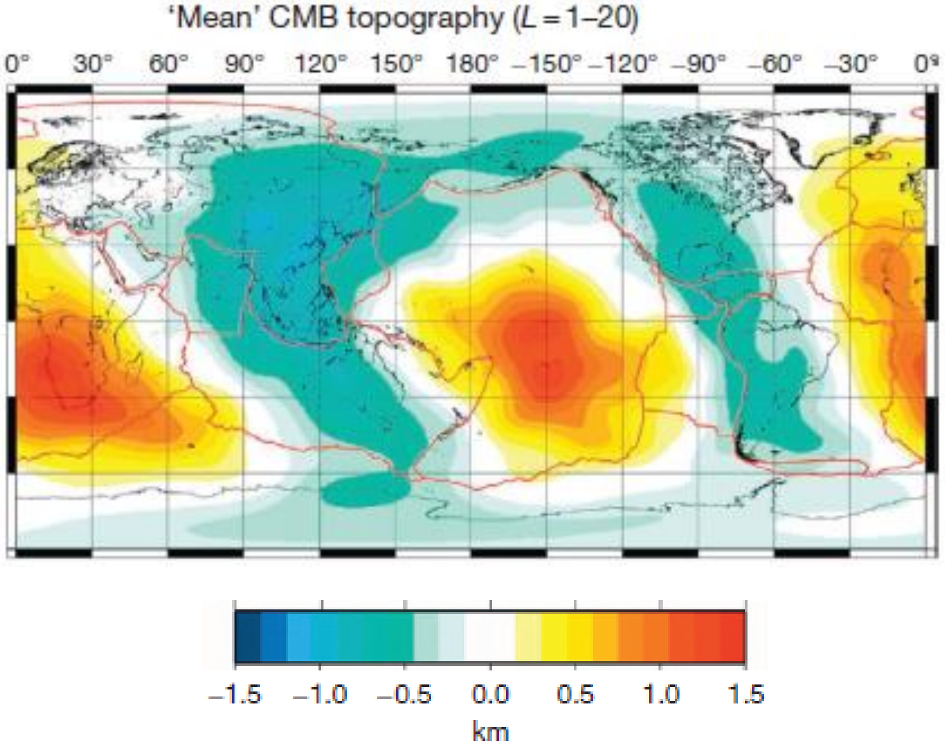

Degree-2 mantle flow pattern in the D” zone

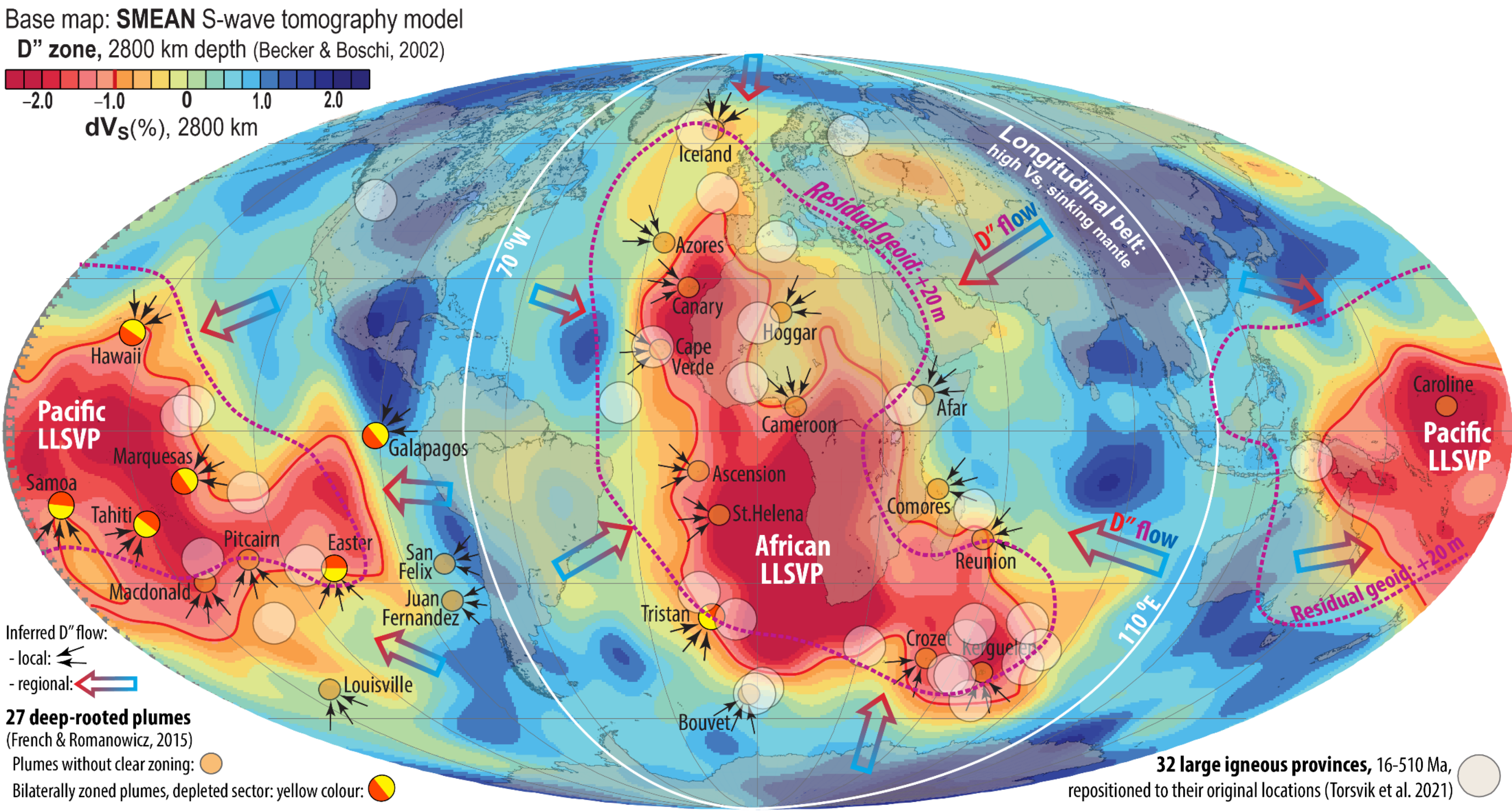

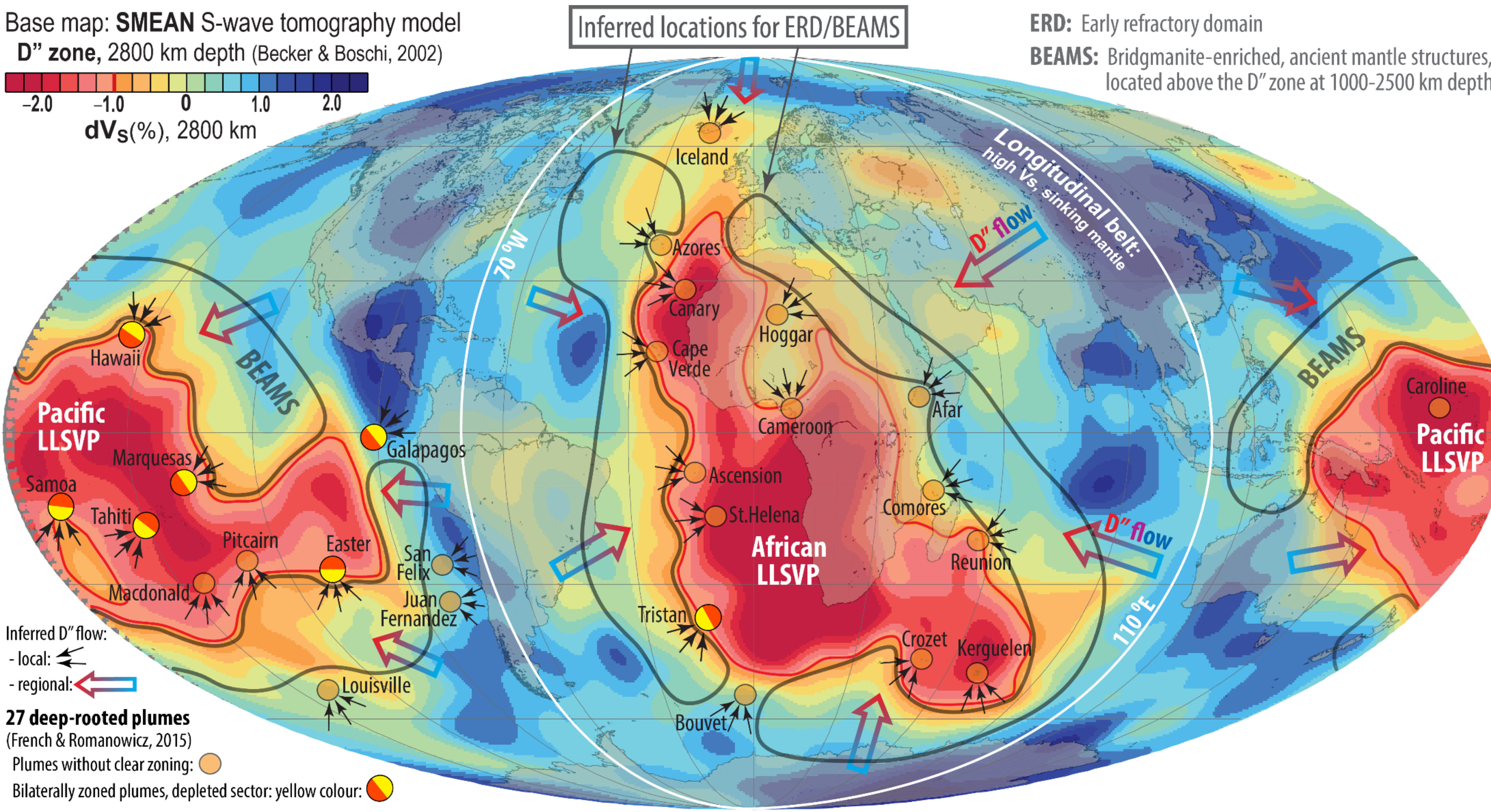

Base map: SMEAN S-wave tomography model
D" zone, 2800 km depth (Becker & Boschi, 2002)
−2.0 −1.0 0 1.0 2.0
dVS(%), 2800 km
Inferred locations for ERD/BEAMS
ERD: Early refractory domain
BEAMS: Bridgmanite-enriched, ancient mantle structures, located above the D" zone at 1000-2500 km depth
Longitudinal belt: high Vs, sinking mantle
D" flow
D" flow
70 °W
110 °E
BEAMS
BEAMS
Pacific LLSVP
Pacific LLSVP
African LLSVP
Iceland
Azores
Canary
Hoggar
Cape Verde
Cameroon
Afar
Ascension
St.Helena
Comores
Reunion
Tristan
Crozet
Kerguelen
Bouvet
Caroline
Hawaii
Marquesas
Samoa
Tahiti
Pitcairn
Easter
Macdonald
Galapagos
San Felix
Juan Fernandez
Louisville
Inferred D" flow:
- local:
- regional:
27 deep-rooted plumes
(French & Romanowicz, 2015)
Plumes without clear zoning:
Bilaterally zoned plumes, depleted sector: yellow colour:

Equatorial section

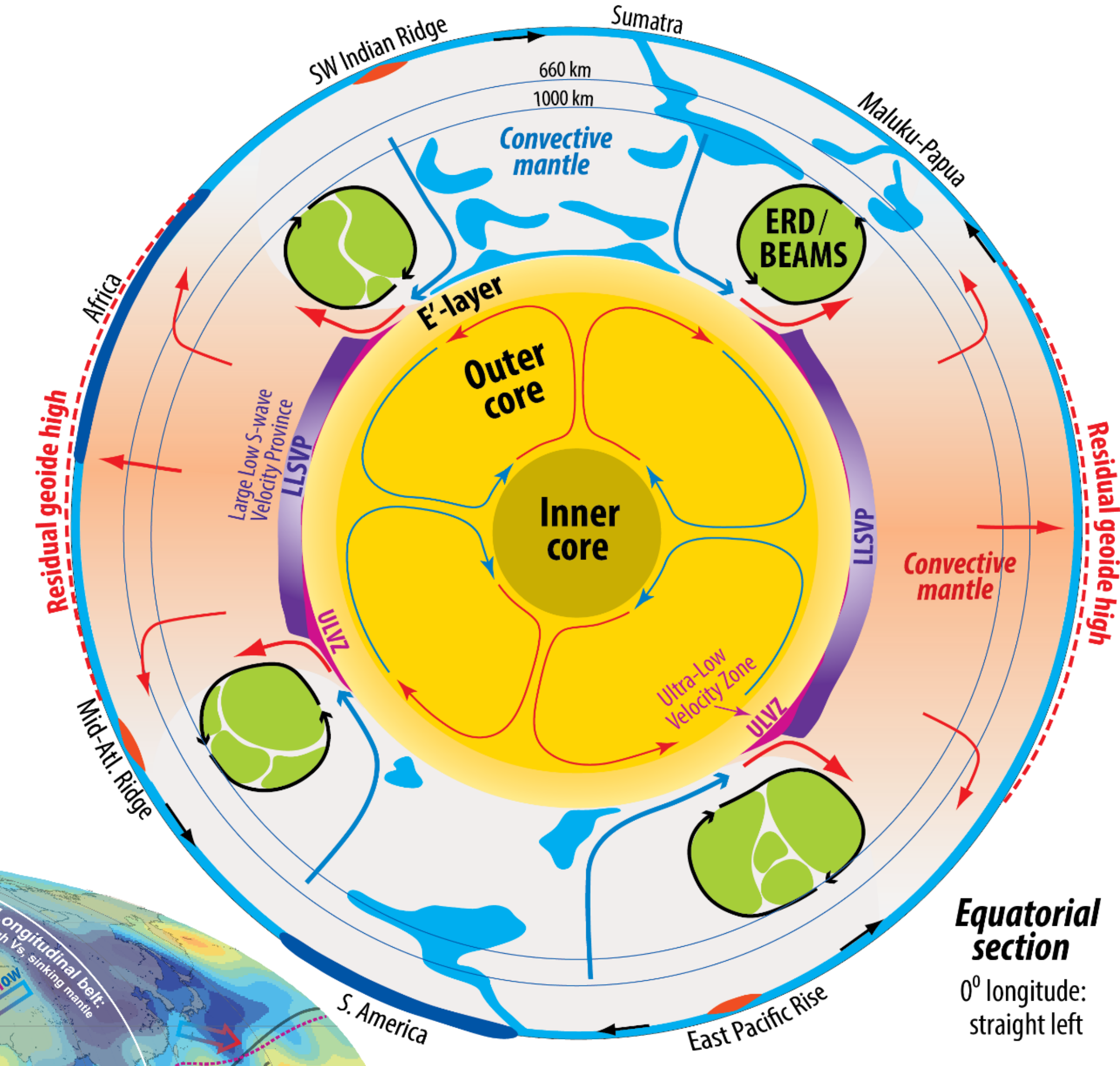

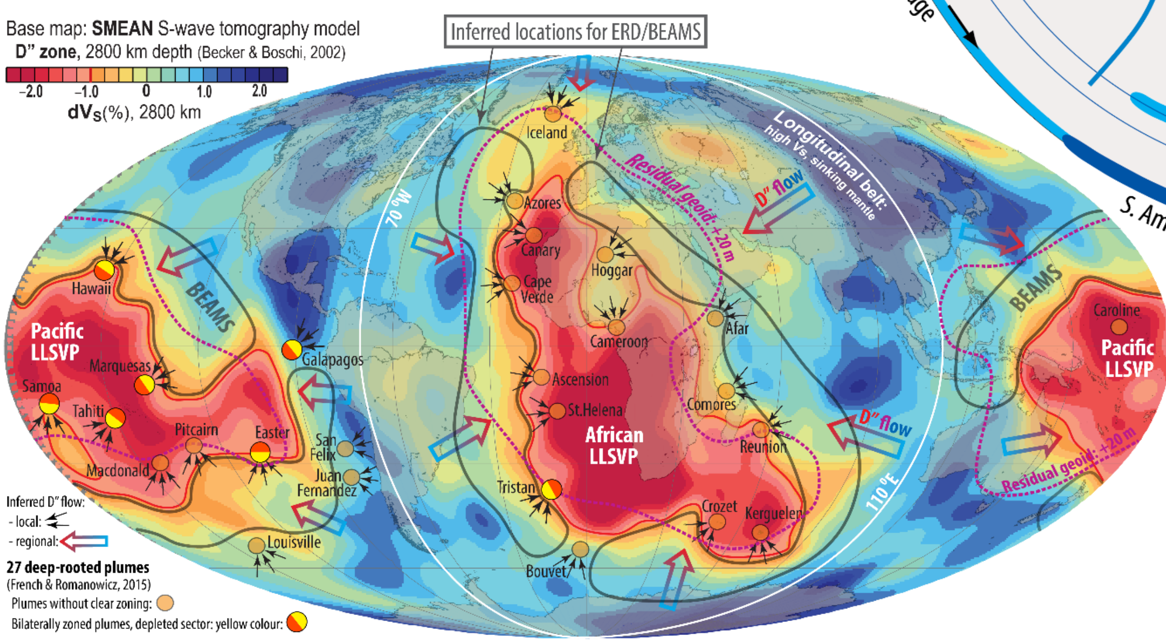

Longitudinal section

The 150ºW-30ºE section (yellow line), intersecting the LLSVPs, is chosen

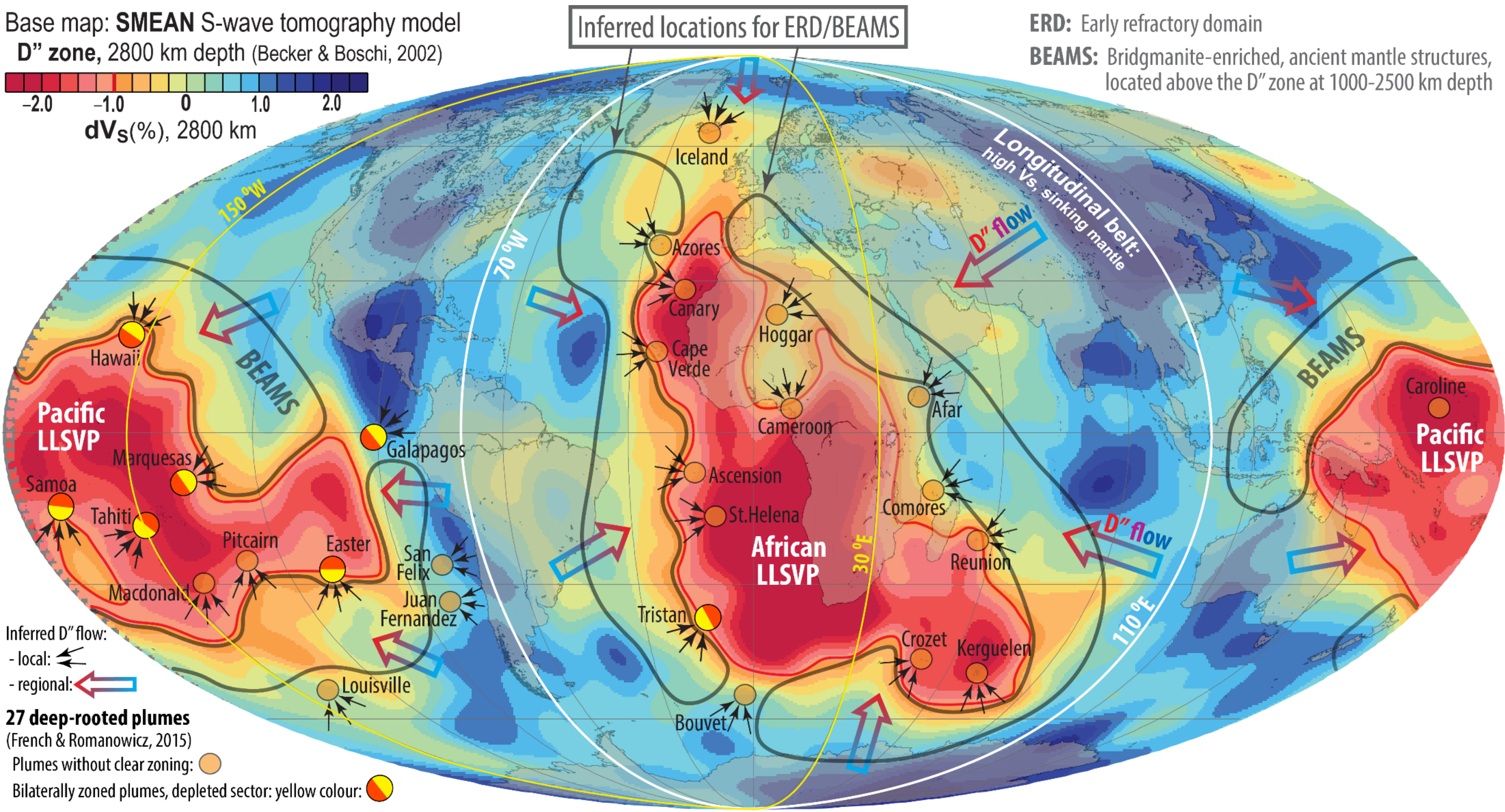

Longitudinal section

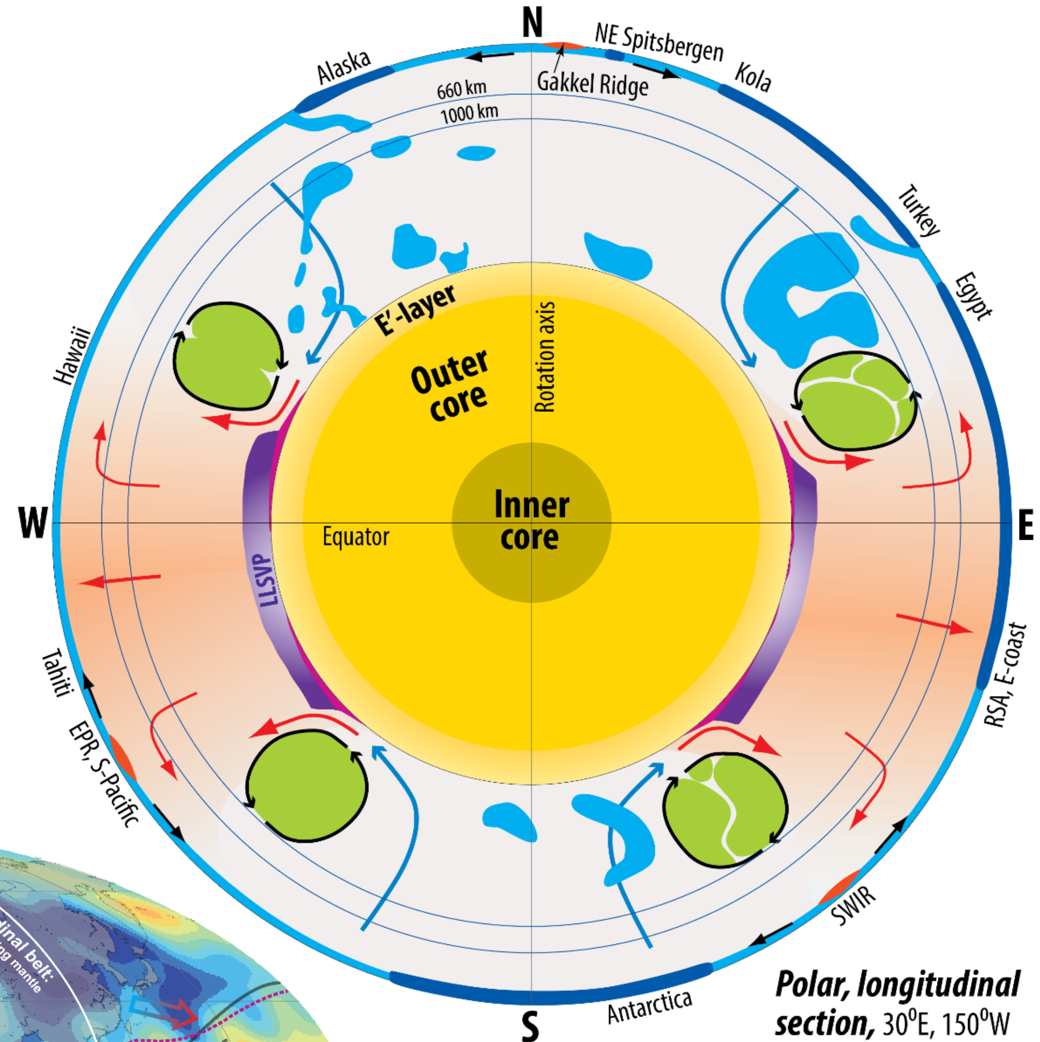

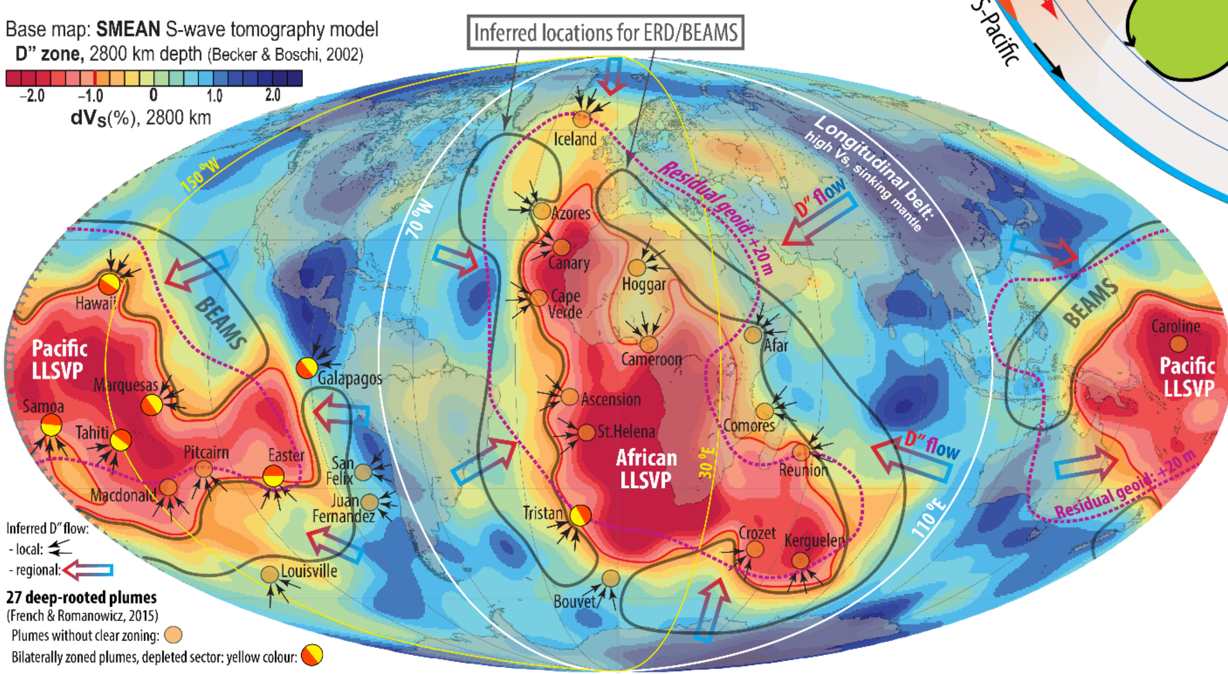

LM viscosity

Increases to 10^{23}-10^{24} Pa s from 660 to ~1500 km depth

Steinberger & Calderwood 2006, PEPI; Marquardt & Miyagi, 2013, N Geosci; Rudolph et al. 2016, Sci

Extreme viscosity decrease in D", due to pbm and CMB-TBL

Amman **et al**. 2010, Nat; Goryaeva et al. 2016; Dobson **et al**. 2019, PNAS)

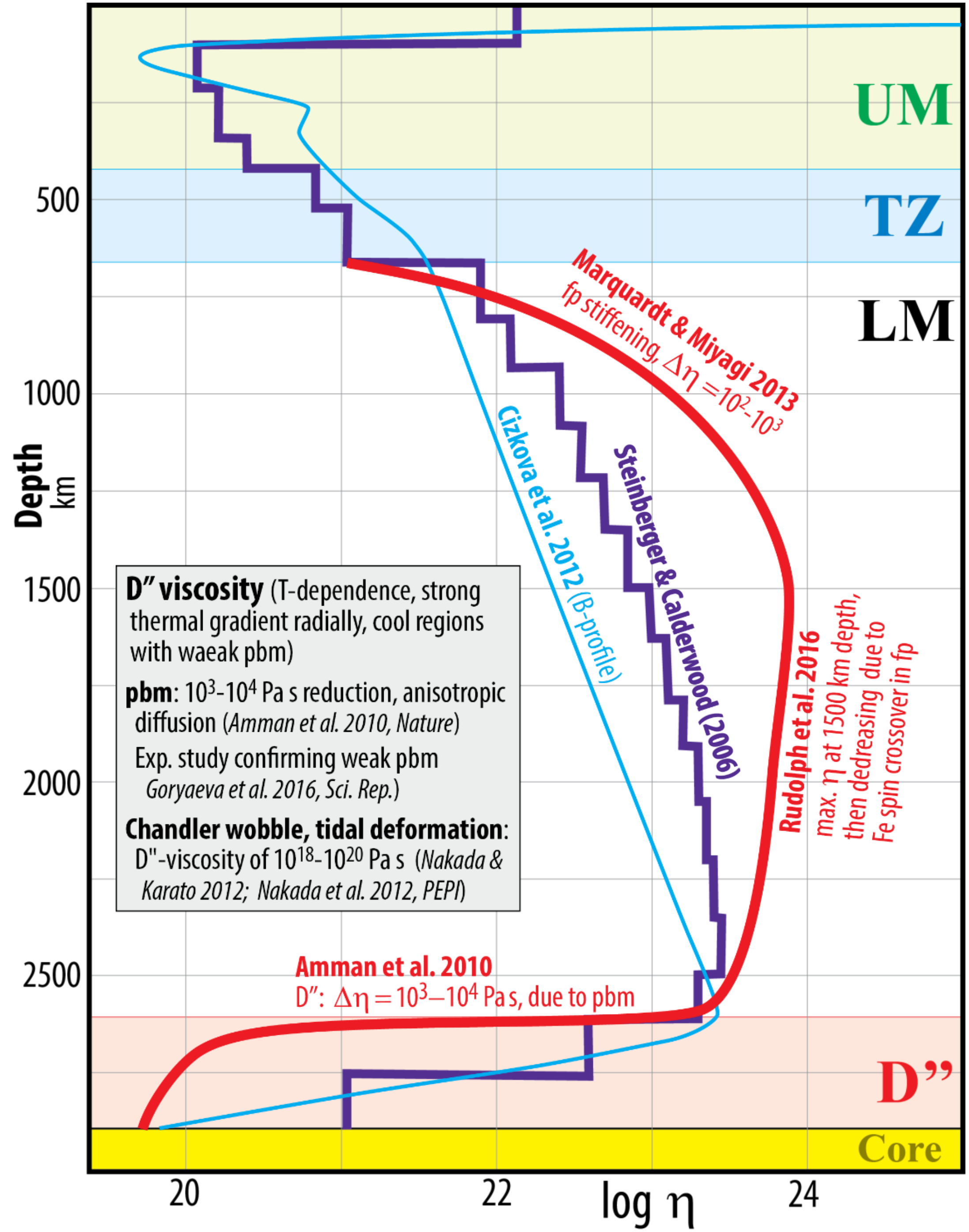

LLSVP base layer **velocity decrease** and density excess

LLSVPs are **mainly restricted** to the lowermost 200-400 km (e.g. Romanovicz 2003, AREPS; Forte et al. 2015. Treat Geophys)

Vs tomography models
Large Vs-amplitudes at the **top** and **bottom** of the mantle

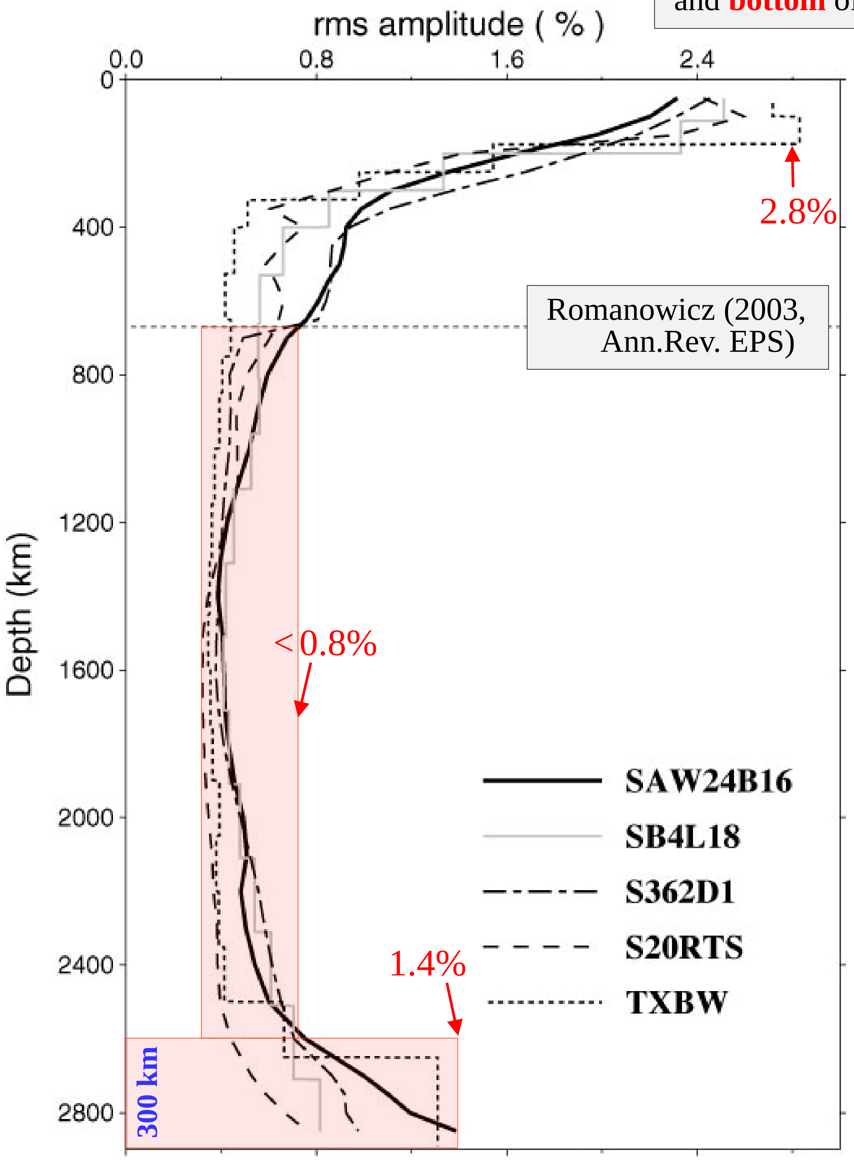

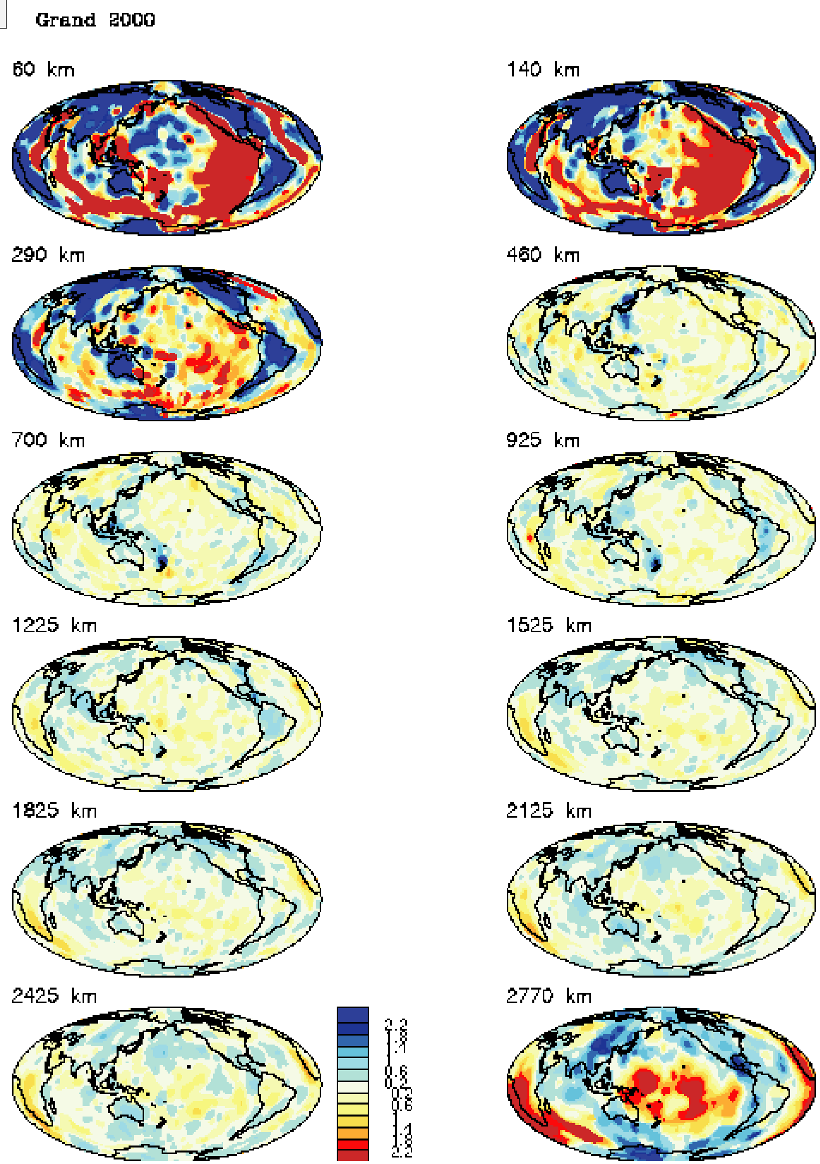

LLSVP base layer velocity decrease and **density excess**

Base-layer Δρ: 1.25% (intrinsic material Δρ: 2.2%, ΔT: 750 K) (Ishii & Tromp 1999, Sci; Moulik & Ekstrøm 2016, JGR; Lau et al. 2017, Nat)

See also: Robson et al. 2021, GJI

Lateral density models, D"

Ishii & Tromp 1999
2850 km depth, range ±1.0%

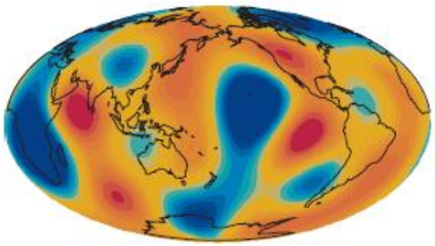

Moulik & Ekström 2016
2800 km depth, scale included

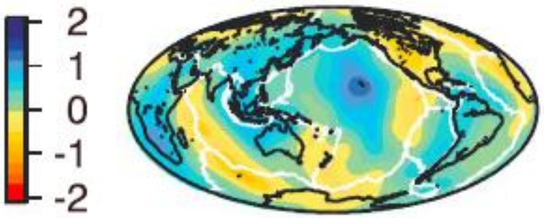

Lau et al. 2016: "Tidal tomography"
2891-2541 km depth (350 km interval above CMB)

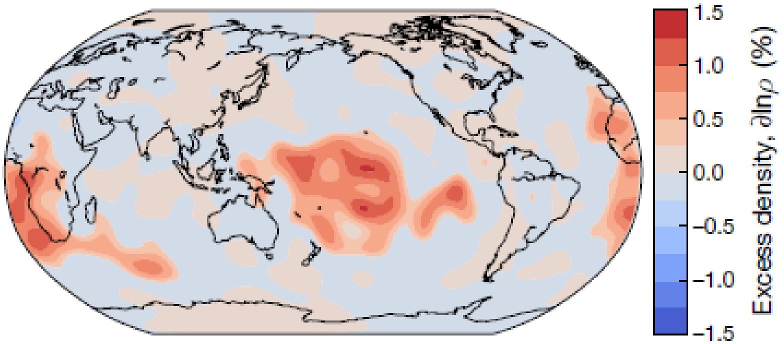

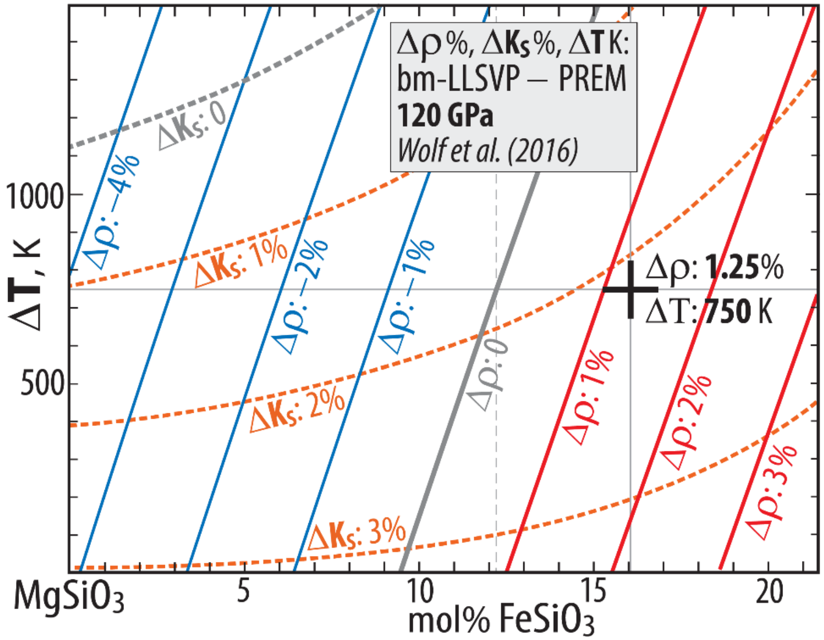

Mineral physics model for bm-dominated LLSVP base layers from Wolf et al. (2016), adopted by Trønnes et al. (2019).

Depth, p: 2620 km, 120 GPa (lowermost 270 km above the CMB)
ΔT: 750 K, Δρ: 1.25%, consistent with Lau et al. 2017.

Intrinsic material $\Delta\rho_{intrinsic}$: 2.2% (wihout the thermal expansion effect)

Presentation available at:

www.nhm.uio.no/english/about/organization/research-collections/people/rtronnes/1/other-lect/sem-mtg/de-sundvollen.pdf

Trønnes-UiO-page → Teaching → other-lect → sem-mtg → de-sundvollen.pptx